Master of Science in Georesources Management

Research Thesis

Bayesian Decision Theory in Structural Geological Modeling

How Reducing Uncertainties Affects Reservoir Value Estimations

Fabian Antonio Stamm

November 1, 2017

Bayesian Decision Theory in Structural Geological Modeling

How Reducing Uncertainties Affects Reservoir Value Estimations

Master of Science Thesis

for the degree of Master of Science in Georesources Management at
RWTH Aachen University
by

Fabian Antonio Stamm

November 1, 2017

Faculty of Georesources and Material Engineering · RWTH Aachen University

RWTH Aachen University

Printed in Germany

RWTH Aachen, Germany

Dated: *November 1, 2017*

Supervisor(s):

Prof. Florian Wellmann, Ph.D.

Prof. Dr. Janos Urai

Abstract

Please pay particular attention to the preparation of your abstract; use this text as a guide. Every master thesis report must be accompanied by an informative abstract of no more than one paragraph (max 300 words). The abstract should be self-contained. No references, figures, tables, or equations are allowed in an abstract. Do not use new terminology in an abstract unless it is defined or is well-known from the literature. The abstract must not simply list the topics covered in the paper but should (1) state the scope and principal objectives of the research, (2) describe the methods used, (3) summarize the results, and (4) state the principal conclusions. Do not refer to the master thesis report itself in the abstract. For example, do not say, "In this thesis we will discuss". Furthermore the abstract must stand alone as a very short version of the master thesis report rather than as a description of the contents. Remember that the abstract will be the first and most widely read portion of the master thesis report. Readers will be influenced by the abstract to the point that they decide to read the master thesis report or not.

Acknowledgements

First of all I want to thank all the people who have participated in this project .. Remember, often more people have (in some way) contributed to your final thesis than you would initially think of....

RWTH Aachen University
November 1, 2017

Fabian Antonio Stamm

Table of Contents

List of Figures

List of Tables

Acronyms

RWTH Aachen University

November 1, 2017

Chapter 1

Methods

The methods utilized in this work are presented in the following chapter. Bayesian analysis and decision theory are introduced. Focus is laid on Bayesian inference, estimation of uncertain values and the use of loss functions in this context. These methods are incorporated in computational modeling of structural geological settings by programming in a Python 3 environment. Central tools for model construction and conduction of the statistical evaluation are GeMpy and PyMC in particular. These are also presented in this chapter.

1-1 Bayesian analysis and decision theory

As implied by the name, the problems and reasoning behind decision-making are examined in the field of decision theory (Berger, 2013). Such decision problems are commonly influenced by parameters that are uncertain. In statistical decision theory, available statistical knowledge is used to gain information on the nature of these uncertainties. (Such uncertain parameters can be considered as numerical quantities.) In order to find the best decision to a problem, it is possible to combine sample information with other aspects such as the possible consequences of decision-making and the availability of prior information on our uncertainties. Decision consequences are expressed as gains in economic decision theory and as losses, which equal negative gains, in statistics. Prior information might be given for example based on experience from previous similar problems or from expert knowledge (see Batvold and Begg). The approach of utilizing priors is known as Bayesian analysis, which is explained in the following (Berger, 2013). (It goes well with decision theory.)

1-1-1 Basic elements

First, some basic elements are to be defined. The unknown (uncertain) quantity influencing decision-making is usually denominated as the state of nature θ (Berger, 2013). Given statistical information on θ in the form of probability distributions, θ is called the parameter. Decisions are also referred to as actions a. The outcome of statistical tests in form of

information or statistical evidence is denoted as y. Loss is defined as $L(\theta, a)$, so $L(\theta_1, a_1)$ is the actual loss incurred when action a_1 is taken while the true state of nature is θ_1 (Berger, 2013). Loss, expected loss and loss functions are explained in detail further below.

1-1-2 Bayesian inference

Bayesian inference is most importantly characterized by its preservation of uncertainty, in contrast to standard statistical inference (Davidson-Pilon, 2015). Probability is seen as a measure of belief for an event to occur. It has been argued by Davidson-Pilon (2015) that this Bayesian approach is intuitive and inherent in the natural human perspective. These beliefs can be assigned to individuals (Davidson-Pilon, 2015). Thus, different and even contradicting beliefs about the probability of an event might be held by different individuals, based on variations and disparities in the information available to each one individual (Davidson-Pilon, 2015).
The initial belief or guess about an event θ can be denoted as $p(\theta)$ (Davidson-Pilon, 2015; De la Varga and Wellmann, 2016). This is used as the so-called prior probability on which Bayesian updating is based. The beliefs about the occurrence of an event are revalued in the presence of additional information, i.e. the observation of new evidence y. These observations are included as likelihoods $p(y|\theta)$. This process of updating results in a posterior probability $p(\theta|y)$ (Davidson-Pilon, 2015; De la Varga and Wellmann, 2016). It is important to note that the prior is not simply discarded but re-weighted by Bayesian updating. It was also pointed out by Davidson-Pilon (2015) that by utilizing an uncertain prior, the potential for wrongfulness of the initial guess is already included. This means that Bayesian updating is about reducing uncertainty in a belief and reaching a guess that is less wrong (Davidson-Pilon, 2015). Bayesian updating is defined by and conducted via the following equation, called the Bayes' Theorem (Davidson-Pilon, 2015):

$$p(\theta|y) = \frac{p(y|\theta)p(\theta)}{p(y)} \propto P(y|\theta)p(\theta) \tag{1-1}$$

1-1-3 Estimation

The resulting posterior distribution can be used to acquire point estimates for the true state of nature θ. Common and simple examples for such estimators are the mode (i.e. the generalized maximum likelihood estimate), the mean and the median of a distribution (Berger, 2013). The presentation of a point estimate should usually come with a measure for its estimation error. According to Berger (2013), the posterior variance is most commonly used as an indication for estimate accuracy. However, it is argued by Davidson-Pilon (2015) that by using pure accuracy metrics, while this technique is objective, it ignores the original intention of conducting the statistical inference in cases, in which payoffs of decisions are valued more than their accuracies. A more appropriate approach can be seen in the introduction of loss and the use of loss functions (Davidson-Pilon, 2015).

1-1-4 Expected loss and loss functions

Loss is a statistical measure of how bad an estimate is, i.e. how much is lost by making a certain decision. Gains are considered by statisticians as negative losses (Davidson-Pilon,

2015). The magnitude of an estimate's loss is defined by a loss function, which is a function of the estimate of the parameter and the true value of the parameter (Davidson-Pilon, 2015):

$$L(\theta, \hat{\theta}) = f(\theta, \hat{\theta}) \tag{1-2}$$

So, "how bad" a current estimate is, depends on the way a loss function weighs accuracy errors and returns respective losses. Two standard loss functions are the absolute-error and the squared-error loss function. Both are simple to understand and commonly used (Davidson-Pilon, 2015).
As implied by its name, the absolute-error loss function returns loss as the absolute error, i.e. the difference between the estimate and the true parameter (Davidson-Pilon, 2015):

$$L(\theta, \hat{\theta}) = |\theta - \hat{\theta}| \tag{1-3}$$

Accordingly, losses increasing linearly with the distance to the true value are returned for respective estimates. This means that all differences between relative errors are weighed equally, no matter whether they are found in the realm of relatively small or relatively large errors (Hennig and Kutlukaya, 2007).
Using the squared-error loss function returns losses that increase quadratically with distance of the estimator to the true parameter value (Davidson-Pilon, 2015):

$$L(\theta, \hat{\theta}) = |\theta - \hat{\theta}|^2 \tag{1-4}$$

This exponential growth of loss also means that large errors are weighed much stronger than small errors. This might come with over-valuation of distant outliers and misrepresentation of magnitudes in distance. Regarding this, the absolute-error loss function can be seen as more robust (Davidson-Pilon, 2015). Both of these standard loss functions are symmetric and

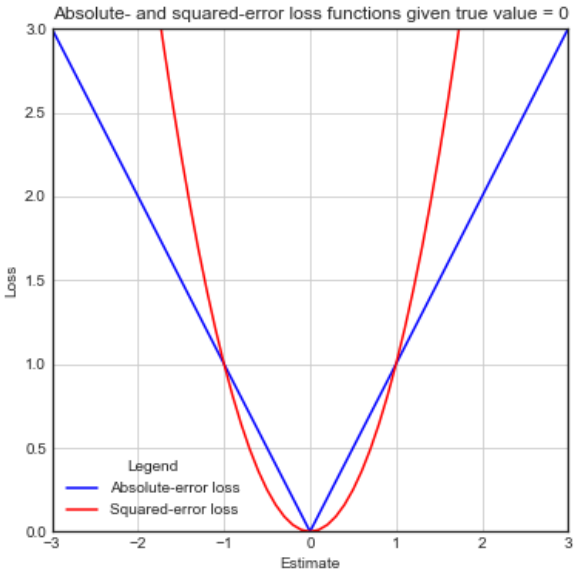

Figure 1-1: Realizations of loss based on the absolute-error loss function (blue) and the squared-error loss function (red) for a determined true value $\theta = 0$.

can be described as objectively aiming at a high precision in estimating the true parameter

value (see Figure 1-1). Davidson-Pilon (2015) and Hennig and Kutlukaya (2007) propose that it might be useful to move away from these type of objective loss functions to the design of customized loss functions that specifically reflect an individual's (i.e. the decision maker's) objectives, preferences and outcomes. Hennig and Kutlukaya (2007) argue that choosing and designing a loss function involves the translation of informal aims and interests into mathematical terms. This process naturally implies the integration of subjective decisions and subjective elements. According to Hennig and Kutlukaya (2007), this is not necessarily unfavorable or "less objective", as it may better reflect an expert's perspective on the situation and contribute to a productive scientific discussion.

The standard loss functions defined above are symmetric, but can easily be adapted to be asymmetric, for example by weighing errors on the negative side stronger than those on the positive side. Preference over estimates larger than the true value (i.e. overestimation) is thus incorporated in an uncomplicated way (Davidson-Pilon, 2015; Hennig and Kutlukaya, 2007). Much more complicated designs of loss functions are possible, depending on purpose, objective and application (Davidson-Pilon, 2015). Some case-specific loss functions are designed in the following chapters of this work.

The presence of uncertainty during decision making implies that the true parameter is unknown and thus the truly incurred loss $L(\theta, a)$ cannot be known at the time of making the decision (Berger, 2013; Davidson-Pilon, 2015). The Bayesian perspective considers unknown parameters as random variables and samples that are drawn from the posterior distribution as possible realizations of the unknown parameter, i.e. all possible true values are represented by this distribution (Davidson-Pilon, 2015). A suitable alternative to the actual loss is to consider a decision's expected loss and to make a decision that is optimal in relation to this expected loss (Berger, 2013).

Given a posterior distribution $p(\theta|y)$, the expected loss of choosing an estimate $\hat{\theta}$ over the true parameter θ (after evidence y has been observed) is defined by the function below (Davidson-Pilon, 2015):

$$l(\hat{\theta}) = E_\theta[L(\theta, \hat{\theta})] \tag{1-5}$$

The expectation symbol E is subscripted with θ, by which it is indicated that θ is the respective unknown variable. This expected loss as defined above, is also referred to as the risk of estimate $\hat{\theta}$ (Davidson-Pilon, 2015).

By the Law of Large Numbers, the expected loss of $\hat{\theta}$ can be approximated drawing a large sample size N from the posterior distribution, respectively applying a loss function L and averaging of the number of samples (Davidson-Pilon, 2015):

$$\frac{1}{N}\sum_{i=1}^{N} L(\theta_i, \hat{\theta}) \approx E_\theta[L(\theta, \hat{\theta})] = l(\hat{\theta}) \tag{1-6}$$

Minimization of a loss function returns a Bayesian point estimate known as Bayes action $\delta^P(X)$, which is the estimate, action or decision with the least expected loss according to the loss function (Berger, 2013). For a unimodal and symmetric absolute-error loss function, the Bayes action is simply the median of the posterior distribution, while using squared-error loss it is the mean (Davidson-Pilon, 2015; Berger, 2013). The MAP (maximum a posteriori) estimate is the minimizing solution for the posterior using zero-one loss (Davidson-Pilon, 2015).

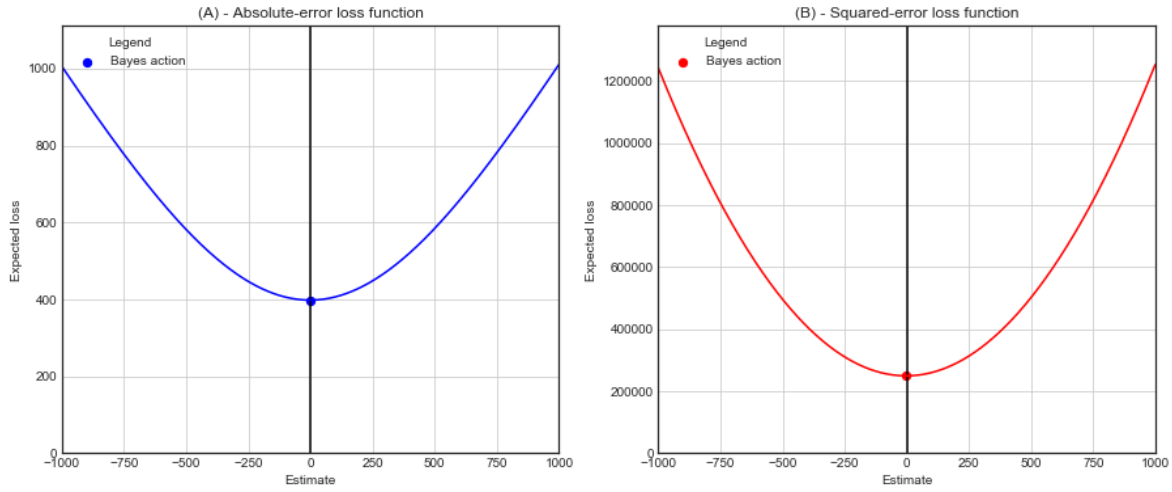

Figure 1-2: Expected loss based on the standard absolute-error loss (A) and squared-loss function (B).

The possibility of more than on minimum also implies that several Bayes actions can exist for one problem (Berger, 2013).
Davidson-Pilon (2015) implemented different risk affinities by simply introducing a risk parameter into the loss function. By using different values for this parameter, it can be represented how comfortable an individual is with being wrong and furthermore which "side of wrong" is preferred by this decision maker (Davidson-Pilon, 2015). This approach to expressing risk-affinities is used the design of loss functions in this work.

1-2 Application in structural geological modeling

In this work, these methods of Bayesian analysis and decision theory are applied in the field of geological structural modeling. The fundamental approach follows closely the research conducted by De la Varga and Wellmann (2016) and builds upon their findings.
According to them, structural geological modeling can be regarded as a forward problem and the elements of Bayesian inference can be specified in this context as follows:

1. **Mathematical forward model (M)**: The connections between parameters θ and observed data y are defined in such mathematical models. According to De la Varga and Wellmann (2016), the realization of a geological model M can be regarded as a direct function of a set of input parameters:

$$M = f(\vec{x}, \phi_i, k_j, \alpha_k, \beta_l), \tag{1-7}$$

where ϕ_i is a function of position $\vec{x}$, more precisely an interpolation function, to which respective additional parameters are given by α_k. Available primary geological information, such as positions of layer interfaces and dips in the subsurface, is represented by k_j. A topological description, such as the relationships between faults and layer surfaces, is given by β_l. An essential aspect of this function is that it allows for a full

automation of the modeling step, so that the consequences of a change in an input parameter are realized directly without the need for any further manual inspection or interaction (Wellmann et al., 2017). The modeling step and respective interpolation used in this work is presented in Section 1-2-2 below.

2. **Model parameters (θ)**: These model-defining parameters can be deterministic or stochastic. In the latter case, they are uncertain parameters to which a probability distribution is assigned. Regarding Equation 1-7 above, these can be any of the factors $\vec{x}$, k_j, α_k and β_l, which define the realization of the forward model over ϕ_i.

3. **Observed data (y)**: This is any type of additional information that can be related to the forward modeling results and might possibly be used to reduce uncertainty. Such data can be gained by measurements and observations, for example by core sampling, well-log analysis or seismic acquisition.

4. **Likelihood functions** $p(y|\theta)$: Links between the previous parameters θ and the additional data y are established by these functions in way that they reflect the likelihood of the parameter states given the observations. They mathematically defined in the same way as probability functions, but are a function of the data y, instead of the parameters θ (De la Varga and Wellmann, 2016).

A fundamental sequence of the inference process was proposed by Gelman et al. (2014), adapted by De la Varga and Wellmann (2016) and is subsequently adjusted for the application in this work as follows:

1. **Setting up a full probability model**: A multi-dimensional joint probability space is to be generated, taking into account the probability distributions of every model parameter θ. A 2D example is illustrated in Figure 1-3.

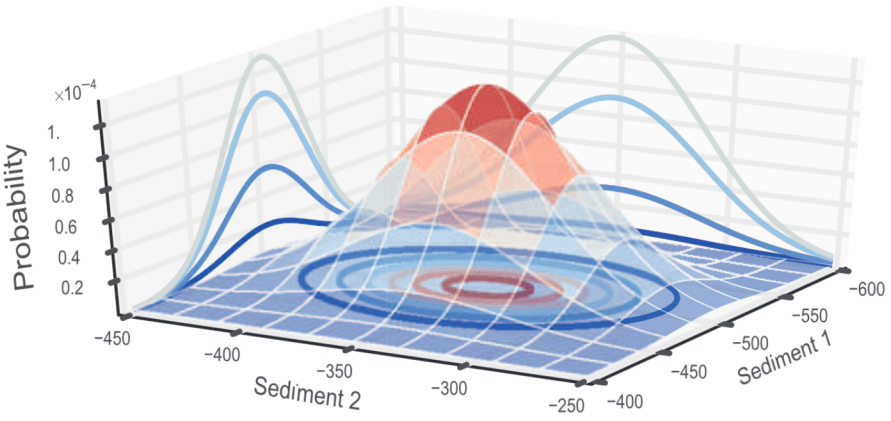

Figure 1-3: Example visualization of a 2D joint probability space generated by two random parameters θ (from De la Varga and Wellmann (2016)).

2. **Conditioning on observed data**: Subsequently, an appropriate posterior distribution $p(\theta|y)$ is to be calculated by conditioning the parameters θ on the observed data y given

the likelihood $p(\theta|y)$. This is the step of Bayesian updating of the belief about the parameter uncertainty given new information. In a chosen model (M), this is achieved by linking parameters and data through deterministic operations which are additionally compared to the likelihood functions. It is pointed out by De la Varga and Wellmann (2016) that any combination of parameter-observation connections is allowed, i.e. not all parameters need to be necessarily connected to all observed data. After all conditional probabilities have been set up, the Bayes Theorem (Equation 1-1) is applied to attain the posterior. However, due to the multi-dimensionality given in geological problems, the use of Markov chain Monte Carlo methods is advised to achieve this as described in Section 1-2-1 below.

3. **Evaluation of the posterior model**: Depending on the aim of the study, a post-processing analysis can be conducted accordingly. De la Varga and Wellmann (2016) focused on the examination of the posterior distributions of the parameters θ and the generated models, particularly regarding information entropy within the model space. In this work, the geological models are assigned an economic meaning by declaring them potential petroleum reservoirs and introducing customized loss functions to reflect the economic interest of decision makers in developing respective resource extraction projects (see Section 1-1-4). Shifts in Bayes actions are considered a measure for the influence of Bayesian inference on decision-making and the significance of additional observations for different decision makers.

1-2-1 Markov chain Monte Carlo sampling (MCMC)

Despite the apparent simplicity of the Bayes Theorem, a direct analytical calculation and exact inference of the posterior distribution $p(\theta|y)$ is rarely possible in non-idealized cases, due to intractability in multi-dimensional spaces (Hoffman and Gelman, 2014; De la Varga and Wellmann, 2016). Thereby arises the necessity to resort to methods of statistical inference approximation. Markov chain Monte Carlo (MCMC) sampling has proven to be a generally applicable and reliable method for exploring multi-dimensional parameter spaces in an intelligent way (Hoffman and Gelman, 2014; Davidson-Pilon, 2015). Gilks (2005) has emphasized the significance of MCMC for the application of Bayesian statistics.

In the ordinary Monte Carlo approach, random independent samples are drawn from a target distribution in order to approximate its shape (Gilks, 2005; De la Varga and Wellmann, 2016). High-dimensional parameter spaces as found in Bayesian applications lead to complex shapes and often make independent sampling infeasible (Gilks, 2005). This can be solved by extending the Monte Carlo principle with a Markov chain, in which every sample iteration of the parameter $\theta^{(t+1)}$ is dependent uniquely on the previous value $\theta^{(t)}$ (Gilks, 2005; De la Varga and Wellmann, 2016).
The general principle of MCMC can be described as follows: Drawing representative samples from an target distribution of unknown shape is based on the conduction of a so-called random walk on the parameter distribution space. T sampling steps are to be performed. The first sampling location is chosen at random. With each subsequent step, a new position is proposed. The new sample value is then related to the previous step. According to a weight defined by the scaled up candidate density of the value, the proposed step is then accepted or rejected. In the case of acceptance, the value is added to the sample trace and the process

is continued from the current location. In the case of rejection, sampling is reverted to the previous accepted step (Schaaf, 2017; De la Varga and Wellmann, 2016). After perform the complete number of T iterations, all accepted sampling locations (i.e. the trace) are returned. The intention behind this concept it to achieve convergence of the sampling algorithm towards areas of high probability (Davidson-Pilon, 2015).
Variations in the way of how new sample steps are proposed and in the acceptance-rejection condition result in different single MCMC sampling methods (Schaaf, 2017; De la Varga and Wellmann, 2016). Various algorithms for random MCMC walks have been developed for over more than six decades and advancements have still been made in recent years. Common examples for such algorithms are the Metropolis-Hastings samplers as devised by Metropolis et al. (1953) and generalized by Hastings (1970). The Gibbs sampler (Geman and Geman, 1984) is another well-known method. For the purpose of this work, an adaptive Metropolis-Hastings sampler is used.
In Metropolis-Hastings methods, each sampling step at iteration t is determined by a candidate probability distribution $q(\theta, \theta^{'})$, from which a proposed sample $\theta^{'}$ is drawn (De la Varga and Wellmann, 2016). The acceptance-rejection condition is defined by the acceptance ratio $a(\theta^{'}, \theta)$:

$$a(\theta^{'}, \theta) = \frac{p(\theta^{'})p(y|\theta^{'})}{p(\theta)p(y|\theta)} \tag{1-8}$$

To ensure a thorough exploration of the probability space, the transition to higher probability densities should not be enforced in every case but selectively. This is assured by relating the acceptance ratio from Equation 1-8 to a random value u from a Uniform distribution $U(0, 1)$ as follows:

$$\theta^{(t+1)} = \begin{cases} \theta^{'} & \text{if } a(\theta^{'}, \theta) > U(0, 1) \\ \theta^{t} & \text{otherwise} \end{cases} \tag{1-9}$$

Thereby, the algorithm assigns high probabilities to high-density points and low probabilities to low-density points, so that the chain state is moved accordingly (De la Varga and Wellmann, 2016).
Metropolis methods are furthermore defined by the step size scale factor that is chosen. While large steps are good for exploration of the space and mixture in the chain, acceptance rates are low. Small steps have better acceptance rates, but lead to slower exploration and convergence of the algorithm (De la Varga and Wellmann, 2016).
For the iterative sampling, Adaptive Metropolis (AM) by Haario et al. (2001) is used in this work. It adapts the traditional Metropolis-Hastings by incorporating the ability of continuous step size tuning during convergence, by taking into account the full information saved along the process. This is achieved by generating a covariance matrix that is updated every iteration. The adaptive nature of the process enables fast convergence for non-linear distributions while maintaining ergodicity Haario et al. (2001); De la Varga and Wellmann (2016). Its suitability for multi-dimensional distribution spaces make it an excellent method for dealing with complex models such as the structural geological models in this work (Schaaf, 2017).
A large enough number of iterations T has to be chosen, so that a reliable and statistically significant exploration of the parameter space is assured. This is primarily dependent on the

rate of convergence towards the true distribution. Considering empirical Bayes methods, in which either priors or likelihoods stem from empirical data, as is assumed for the models in this work, convergence can be expected to be reached almost immediately. However, for high dimensional problems more iterations are required, in order to ensure an accurate representation of posterior distributions (Wellmann et al., 2017). Different realizations of the full 3D geological model are then constructed on the basis of the resulting posterior distributions, using an implicit modeling step described in the following.

1-2-2 Structural geological forward modeling

Performing forward modeling in the context of structural geology requires the use of a suitable modeling step M (see Equation 1-7). For the application in a probabilistic setting, the method should enable fully automatic reconstruction of the model, when parameters are changed. The application in this work follows the example of De la Varga and Wellmann (2016) and relies on the use of implicit interpolation for geological modeling, a method developed and elaborated by Lajaunie et al. (1997) and Calcagno et al. (2008).
This implicit method relies on the interpolation of a potential field scalar function $T(\vec{x})$ of any point $\vec{x}$ in a 3D space, and thus reflects the geometry of geological structures (Calcagno et al., 2008). Modeling $T(\vec{x}$ is achieved by cokriging that regards two forms of data: (i) contact points on geological interfaces through increments of the potential field $T(\vec{x}) - T(\vec{x}^{'})$ and (ii) orientation data as gradients, i.e. partial derivatives of the potential field $\delta T(\vec{x})/\delta u_\beta$ in each directon u (Calcagno et al., 2008). The respective estimator is defined as follows:

$$T(\vec{x}) - T(\vec{x_0}) = \sum_{\alpha=1}^{M} \mu_\alpha (T\vec{x_\alpha} - T(\vec{x}_\alpha^{'})) + \sum_{\beta=1}^{N} \nu_\beta \frac{\delta T}{\delta u_\beta}(\vec{x}_\beta), \tag{1-10}$$

where $\vec{x_0}$ is an arbitrary origin, M and N are the total number of data points and partial derivatives respectively, and their relative contributions are weighed by the factors μ_α and ν_β. Furthermore, T is assumed to be a random function defined by polynomial drift and a stationary covariance $K(h)$ (Calcagno et al., 2008). The use of a cubic covariance model is suggested by Calcagno et al. (2008), based on the results from studies conducted by Aug (2004) and Chilès et al. (2004). Resulting potential fields can be used to describe geological interfaces as iso-surfaces in any kind of 3D geometry (Calcagno et al., 2008). Fault geometries can be interpolated analogously. These can be infinite in the 3D space, interrelated in a fault network or finite. To account for the effect of faults on geological layers, discontinuous potential fields are created by applying discontinuous drift functions in the cokriging system. Additionally, geological rules allow for the representation of several types of interactions between sets of geological layers (Calcagno et al., 2008).
It is pointed out by Calcagno et al. (2008), that this method is particularly appropriate for cases in which knowledge about the geology is only given a sparse locations and is thus applicable for a wide variety of typical problem in geological settings. Its suitability for this work is furthermore emphasized by the possibility to modify the topology-defining geological pile to achieve different geometric realizations without altering the data. The model can thus be updated in the face of new data or interpretations (Calcagno et al., 2008).

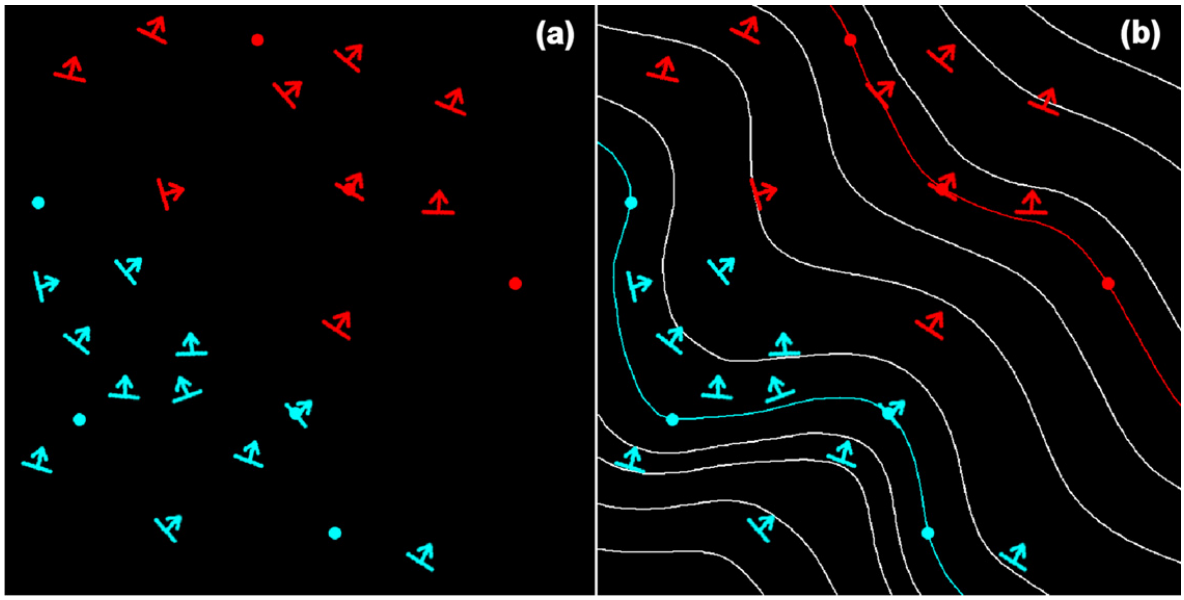

Figure 1-4: Illustration of the concept of interpolating to attain a poentail field. The original data is depicted in (a), with contact points as dots and orientation measurements indicated by arrows. Colors represent respective assignments to different formations. An accordingly calculated potential field is shown in (b) (from Calcagno et al. (2008)).

1-2-3 Numerical computational implementation via Python, GemPy and PyMC

Bayesian analysis can be conducted using probabilistic programming (Salvatier et al., 2016). The implicit method of forward geological modeling, described above, is to be embedded in such a framework. For doing so, the programming language of choice in this work is Python. The merits of Python have been pointed out by Behnel et al. (2010); Salvatier et al. (2016); Langtangen (2008). Development is facilitated by an expressive but concise and clean syntax that is easy to learn. Python is dynamic, compatible with multiple platforms and offers good support for numerical computing. Integration of other scientific libraries and extension via C, C++, Fortran or Cython are easily possible (Behnel et al., 2010; Salvatier et al., 2016; Langtangen, 2008). Python is thus a straightforward tool for the implementation of central components of Bayesian analysis, such as custom statistical distributions and samplers (Salvatier et al., 2016).

The 3D geological modeling step in this work is implemented using GeMpy, an open-source, Python-based software that is able to generate and visualize complex 3D structural geological models based on the potential field interpolation method elaborated in Section 1-2-2 (De la Varga and Schaaf, 2017). Its design allows for its application in a probabilistic setting, particularly by coupling it with PyMC as elaborated below. At the time of writing this, GemPy is still under development (version 0.995), but is already functioning for the purpose of this work.

For conducting the Bayesian analysis and embedding the geological modeling step in a probabilistic modeling framework, GemPy is combined with PyMC. This Python library was developed for conducting Bayesian inference and prediction problems in an open-source probabilistic programming environment (Davidson-Pilon, 2015; Salvatier et al., 2016). Different

model fitting techniques are provided in PyMC, such as the *maximum a posteriori* (MAP) method and several (MCMC) sampling methods, including the Adaptive Metropolis explained in Section 1-2-1 (Salvatier et al., 2016). The components which are used to construct a statistical model, are represented by *Deterministic* or *Stochastic* variables in PyMC. The values of *Deterministic* variables are completely dependent on its parents' values, as defined by a respective mathematical function (Salvatier et al., 2016). *Stochastic* variables are used to represent uncertain parameters θ or observed stochastic variables as likelihood functions $p(y|\theta)$ (Salvatier et al., 2016; De la Varga and Wellmann, 2016). Complex mathematical relations between *Stochastic* variables can be described through *Deterministic* variables (De la Varga and Wellmann, 2016). Futhermore, PyMC allows for the creation of own object definitions inheriting from the class descriptions of these two variable types.
Salvatier et al. (2016) point out that the development of PyMC is continuing, as the inclusion of further tools is planned for future updates.

1-2-4 Bayesian hierarchical networks

1-3 Model evaluation

1-3-1 Economic significance and reservoir system valuation

In this work, the generated structural models are to be assigned an economic significance in order to approach a real setting, in which hypothetical actors could have an interest in taking a decision, and thus, to evaluate the influence of the Bayesian inference of the decision-making process. Changes in Bayes actions are considered as a measure for this effect. For this purpose, it is assumed that a hydrocarbon reservoir system is represented by each geological model realization. Such hydrocarbon systems are typically comprised of:

1. A kerogen-rich **source rock** which produced and emitted hydrocarbons during its burial history, given sufficient heating (Dolson, 2016a) These are typically organic-rich sedimentary rocks, shales in particular. For the purpose of this work, it is assumed that a suitable source rock is present and hydrocarbons expulsion took place after the formation of any trap-defining structures in our geological models.

2. A **pathway** that allows expelled oil and gas to migrate upwards through the subsurface from the source rock into potential reservoir formations (Dolson, 2016a). This condition is also assumed to be given in our model. Basement formations in the geological model are simply defined as permeable.

3. **Seal** formations that are able to halt hydrocarbons on their migration pathway as top, lateral and possibly bottom seals (Dolson, 2016a; Sorkhabi and Tsuji, 2005). Such sealing is generally defined by a reduction of pore space geometry relative to migration energy. Sealing is thus defined primarily by changes in stratigraphical composition to low porosities and micro-sized pore throats. These are characterized by a high capillary entry pressure able to resist the buoyancy pressure of hydrocarbons. This capillary pressure is also the main controlling factor for seal capacity. Lithologically, seals are most commonly comprised of shales, siltstones, tight carbonates, evaporites and salts

(Dolson, 2016a; Sorkhabi and Tsuji, 2005; Dolson, 2016b). An additional factor to sealing is posed by the presence of faults. Fault zones may possess significantly higher or lower permeabilities then surrounding rock formations which means that they may serve as fluid flow conduits or migration barriers respectively (van der Zee et al., 2003; Sorkhabi and Tsuji, 2005). The possible influence of faults on structural hydrocarbon traps is elaborated in further detail below. For the model in this work, the reservoir cap rock is assumed to be a shale.

4. Suitable **reservoir formations**, in which these hydrocarbons volumes can be stored. For this, a suitable percentage of void space in a rock formation, i.e. a sufficiently high porosity, is required. Further significant factors are the connectivity of the porosity through pore throats, as well as pore geometry and resulting permeability (Dolson, 2016a; Sorkhabi and Tsuji, 2005). The larger the pore throats, the easier it is for fluids to migrate in a rock. Typical reservoir rocks are sandstones and carbonates, but even normally tight lithologies might serve as reservoirs, if they are fractured (Dolson, 2016a). In the models of this work, reservoir formations are assumed to be conventional sandstones.

5. A **trap** resulting from an appropriate reservoir-seal sequence and a three-dimensional geometric closure. Regarding a top view on a structural relief, closure is generally defined by any intersection of a structural contour and the seal, that is closed on both sides (Dolson, 2016a; Sorkhabi and Tsuji, 2005). A point at which a contour fails to close is referred to as "spill point". The maximum column depth to which a trap can be filled, and ultimately its maximum volume, is defined by this spill point. A trap that contains hydrocarbons down to the spill point is thus referred to as "filled to spill". traps can also be "filled to seal capacity" when the seal capacity is exceeded by the buoyant pressure of a fill column of greater height. Lower accumulations can also result from insufficient migration, i.e. low charge volumes of oil or gas in the first place. Such a trap is referred to as "charge limited" (Dolson, 2016a). Many different types of traps, in which hydrocarbons can accumulate, are possible. A common trap type is a structural four-way closure, i.e. as reservoir-seal system that was folded into closed anticlines, often resembling a dome and is thus predominantly defined by the structural closure relief and the cap rock sealing capacity. Such a trap type can be considered to be closed, as the reservoir surface contours are closed in a circle or oval around a relief high. Closure can also be given through the intersection of a fault with the seal (Dolson, 2016a). Two common examples are illustrated in Figure 1-5.

The presence of a fault in the reservoir-seal sequence can have different impacts on trap closure and the volume of a hydrocarbon accumulation. This is mainly defined by the transport properties of a fault, i.e. in which way it behaves as a seal or flow conduit respectively. Cases might range from complete fault sealing to complete leakage along a fault zone. More complex in-between cases are possible, such as faults that leak across, but are sealed along their plane. This ultimately defines the depth to which a trap may be filled and whether this point is controlled by a point of leakage on the fault plane or a spill point related to the remainder of the 3D structural closure. Another decisive aspects to consider, it the nature of juxtapositions across the fault, especially regarding the possibility of cross-fault leakage (van der Zee et al., 2003). This is summarized in Figure 1-6.
The transport properties of a fault zone are primarily defined by the internal structure and

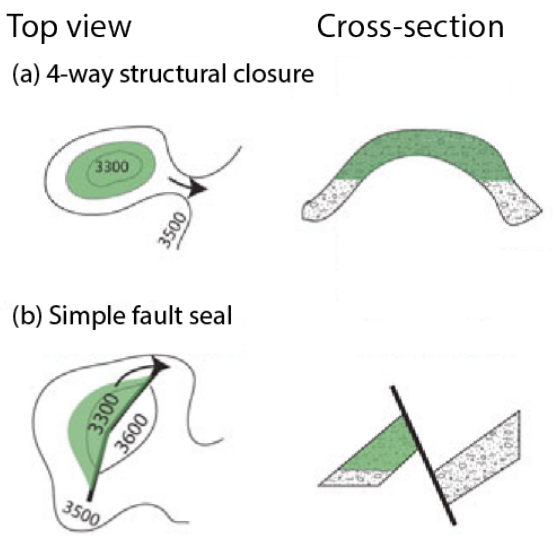

Figure 1-5: Conceptual examples of a dome-shaped four-way-closure and a simple fault trap from top view (relief contour) and cross section perspective (modified from Dolson (2016a).)

composition of its fault gouge. Fault gouge properties and ultimately the variation in permeability in the fault zone is primarily dependent on clay content. Clay smearing has thus been a central topic of research surrounding fault sealing (see Lindsay et al. (1993); Yielding et al. (1997); van der Zee et al. (2003); van der Zee and Urai (2005); Schmatz et al. (2010). It generally is defined as all processes that lead to the incorporation of clay from the wall rock (e.g. a shale as seal) into the fault zone (van der Zee et al., 2003; Vrolijk et al., 2016). Clay smearing can be described using different equations, such as the Shale Smear Factor (SSF) and the Shale Gouge Ratio (SGR) (Lindsay et al., 1993; Yielding et al., 1997; Vrolijk et al., 2016). The SSF provides a simple conceptual approach to assessing the clay smearing on a fault plane, dependent on ratio of fault throw magnitude D to displaced shale thickness T (Lindsay et al., 1993; Yielding et al., 1997; Yielding, 2012) (see Figure 1-7):

$$SSF = \frac{D}{T} \tag{1-11}$$

It has been observed, that as the displacement and thus the ratio increases, a critical value SSF_c will be reached, at which the clay smear is breached and no longer continuous. Initial observations by Lindsay et al. (1993) indicated this threshold to be $SSF_c = 7$. However, the critical value was later suggested to be scale-dependent and smaller for thick clays dispalced by large faults (Yielding, 2012). Færseth (2006) reported that for such scales, including fault throws greater than 100 m, clay smear conitinuity can be expected for $SSF \leq 4$. Any larger values come with a decrease in confidence (Færseth, 2006).
A critical review of the respective research published over the last four decades was recently presented by Vrolijk et al. (2016).
The 3D structural model in this work (see Section 1-6-1) is designed in a way that a potential conventional hydrocarbon trap is included in the form of anticlinal folding combined with normal faulting of a reservoir-seal sequence. Results from modeling are to be evaluated in a way that respective estimations on the basis of loss functions can be conducted, i.e. Bayesian

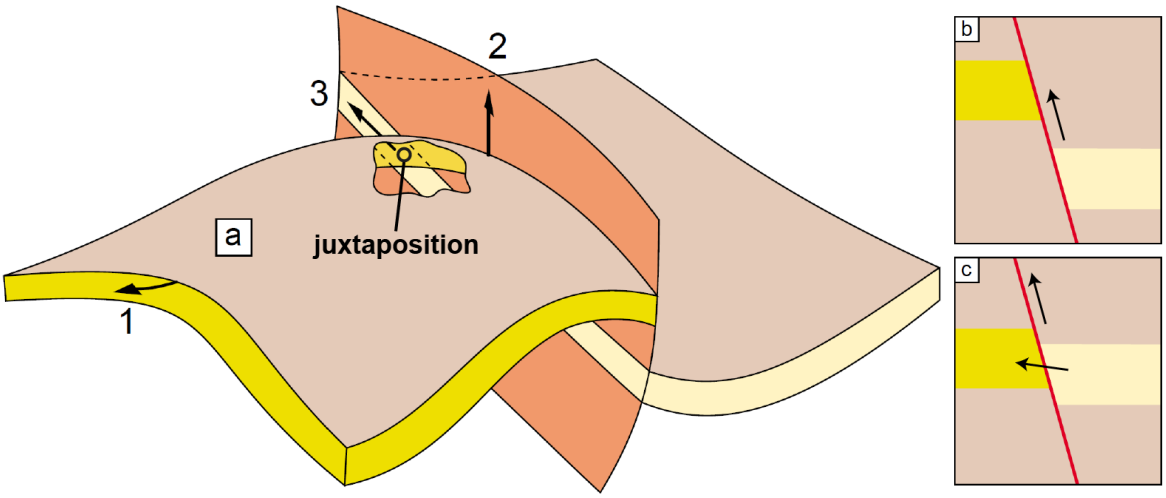

Figure 1-6: In (a), a structural trap resulting from the combination of 4-way anticlinal closure and a simple normal fault is illustrated. The two reservoir layers in both sides are juxtaposed, so that the hydrocarbon accumulation potential is controlled by three points of possible leak pathways: (1) the anticlinal spill point, (2) leakage upwards along the fault and (3) leakage across the fault enabled by the juxtaposition. Possibilities (2) and (3) depend on the transport properties of the fault zone, i.e. potential fault sealing. Given leakage along the fault (2), that size volume would be reduced to a small relatively small volume solely defined by the 4-way closure down to maximum contact of the reservoir-seal boundary with the fault plane. In case (b), the reservoirs are not juxtaposed and thus laterally sealed. Fault-related leakage can thus only occur along the plane. Leakage along and across the fault is enabled by the juxtaposition in (c) (modified from van der Zee et al. (2003)).

decision theory is applicable. In the typical petroleum industrial setting, the main question is one of how much of the resource can be produced and how high the return on investment will be (Dean, 2007). Thus, several of the factors named above are to be considered to attain a calculable volume of the structural trap which can further be economically interpreted using the approaches presented below.

1-3-2 Original oil-in-place and recoverable volumes as value measures

Before pressure and production tests have been conducted (i.e. before production has started), volumetric estimation is the only approach to assess the amount of hydrocarbons in place in a reservoir. From this value, recoverable reserves can be estimated based on an estimated recovery factor (Dean, 2007).
Oil-in-place and gas-in-place volumes are calculated based on:

1. Subsurface rock volume containing hydrocarbons. This is mainly defined by thickness and areal extend of the accumulation.

2. Weighted average effective porosity of the reservoir rock.

3. Water saturation in the reservoir rock.

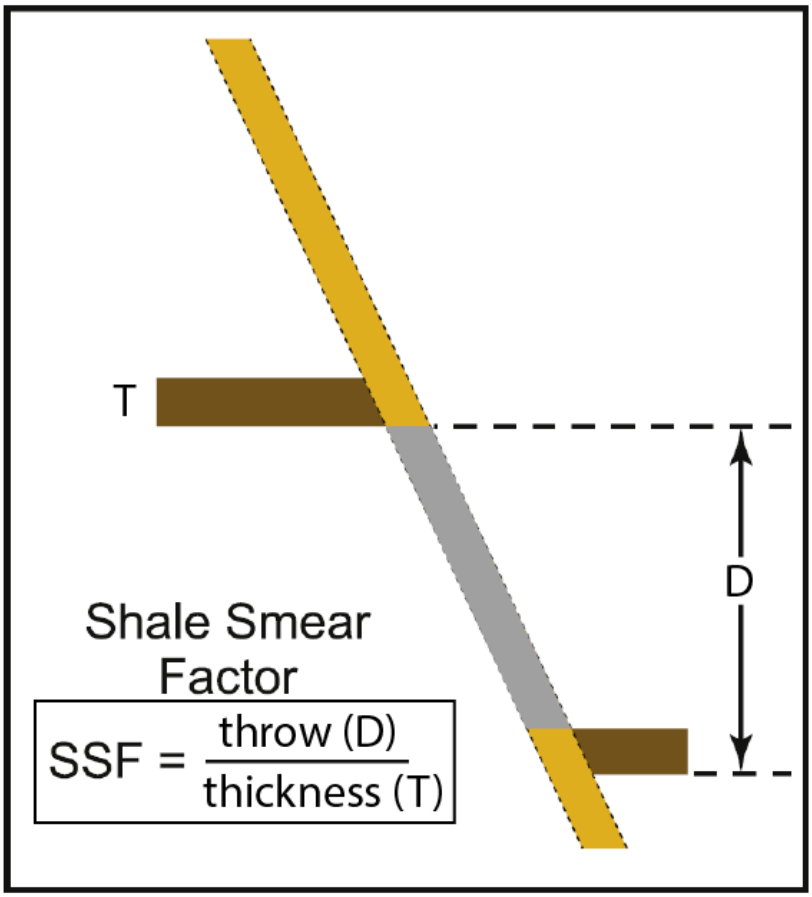

Figure 1-7: Conceptual fault section illustrating the SSF approach to assess shale smear potential (modified from Vrolijk et al. (2016).)

4. Hydrocarbon fluid properties (Dean, 2007).

As the cases used in this work are purely artificial, a pure oil accumulation is assumed. Using the factors listed above, the respective equation for original oil-in-place ($OOIP$) is formulated as follows:

$$OOIP = A * h * \phi * (1 - S_W) * 1/FvF \tag{1-12}$$

Where $OOIP$ is returned in m. The hydrocarbon-filled rock volume is defined by the drainage area A in m and the net pay thickness h in m. Porosity ϕ and water saturation S_W (interstitial water) are given in fraction of the rock volume. A dimensionless factor for the change in oil volume between reservoir conditions and standard conditions at surface is represented by the formation volume factor FvF. Thus, shrinkage of the oil volume brought to the surface is determined by $1/FvF$ (Dean, 2007).
Subsequently, the effectively recoverable oil volumes (ROV) can be calculated by multiplying the $OOIP$ with a recovery factor RF:

$$ROV = OOIP * RF = A * h * \phi * (1 - S_W) * 1/FvF * RF \tag{1-13}$$

the recovery factor is influenced by a number of fluid properties, such as viscosity, density, solution oil/gas ratio and the formation volume factor. Thus, it is difficult to estimate (Dean,

2007). Globally, the ultimate average recovery factor for oil fields is about 35% (Labastie, 2011). For gas accumulations, however, recovery factors range typically between 70 and 90% (Dean, 2007).
The models in this work are completely hypothetical and not based on real data. The inputs to these equations can thus be chosen arbitrarily to test the applied methods. However, to come to significant conclusion, it makes sense to utilize values that approximately represent real possible scenarios. Furthermore, as 3D geological structures are modeled here, the hydrocarbon-filled rock volume ($A * h$ in Equations 1-12 and 1-13) is defined by every realization of the uncertain geological model. The rock volume is thus an uncertain factor. Remaining factors can be implemented deterministically or as uncertain values, too. For most factors, it seems most suitable to define a normal distribution around a known typical value or global average, as it will return a high probability for common scenarios and occasionally produce cases of rare, more extreme values. (INSERT WHAT IS CHOSEN IN THE END - MAYBE MORE SENSE TO TAKE FIXED VALUES FOR THE FACTORS THEN RV, SO THAT ITS INFLUENCE IS CLEAR; THEN MAYBE INCLUDE POROSITY? OR COMPARE BOTH POSSIBILITIES?).
Consequently, $OOIP$ and ROV calculations represent the step following and using the results from computing the geological model, so that the realizations are assigned values that can be interpreted from a perspective of economic interest. The resulting values from numerous model runs are used as a base probability distribution for the true value, on which loss function estimation can be applied as described in Section 1-1-4. $OOIP$ and ROV are applicable in a 3D setting, the 1D geological model introduced below in Section 1-5, however, requires the use of an abstract valuation system that is explained in Section 1-5-3.

1-4 Designing a case-specific loss function

As explained before in Section 1-1-4, the standard symmetric loss functions provide objectively good estimators minimizing expected loss by returning the median or mean respectively. However, assigning an economic notion to our model and assuming the case of an actor or decision maker in any field, naturally necessitates the consideration of preferences, interests and the overall subjective perspective such an individual or for example a company might have. Further constraints, properties and factors can also be specific to the field, industry or generally to the problem at hand. Consequently, the design of a more specific non-standard and possibly asymmetric loss function might be required, so that an adapted Bayesian estimator can be found. One that includes subjective aspects and difference in weighting of particular gains or losses, arising from an actor's inherent preferences and the environment in which the actor has to estimate or make a decision. In the face of several uncertain parameters, a perfectly true estimate is virtually unattainable. However, an attempt can be made to design a customized loss function that returns a Bayesian estimator involving the least bad consequences for an individual in a specific environment. Assuming the reservoir setting case and valuation methods introduced in Section 1-3-1), such a customization attempt is made and explained step by step in the following. (SOURCES?)
For the purpose of estimation, it makes sense that one of the standard loss functions is chosen as a basis and a customized loss function is developed from there. The absolute-error loss seems most appropriate for this case of hydrocarbon reservoir value estimation. Ideally, an actor would like to know the exact true value of interest, say the OOIP, so that investments or

resources can be allocated appropriately in order to acquire economic gains. This allocation is the decision to be made or action to be taken. Deviations from the unknown true value in the form of over- and underestimation bring about an error and loss accordingly. In this case, it is assumed that investments increase linearly with linear growth in the value of the resource. For this reason, the absolute-error loss function is favored here over the squared-error loss function. It is chosen as the base function to which further development steps refer, based on mostly logical case-specific assumptions:

1. **Step I**: The standard symmetrical absolute-error loss function is chosen as a starting point for further customization steps:

$$L(\theta, \hat{\theta}) = |\theta - \hat{\theta}| \tag{1-14}$$

2. **Step II**: Considering the development of a hydrocarbon reservoir, it can be assumed that over-investing is worse than under-investing. Overestimating the size of an accumulation might for example lead to the installation of equipment or facilites that are actually redundant or unnecessary. This would come with additional unrecoverable expenditures. Consequences from underestimating, however, may presumably be easier to resolve. Additional equipment can often be installed later on. Hence, overestimation is weighted stronger in this loss function by multiplying the error with an overestimation factor a $(= 1.25)$:

$$L(\theta, \hat{\theta}) = |(\theta - \hat{\theta})| * a \tag{1-15}$$

3. **Step III**: The worst case for any project would be that its development is set into motion, expecting a gain, only to discover later that the value in the reservoir does not cover the costs of realizing the project, resulting in an overall loss. A petroleum system might also turn out to be a complete failure, containing no value at all, although the actor's estimate indicated the opposite. Here, this is referred to as worst case or fatal overestimation. A positive value is estimated, but the true value is zero or negative. This is worse than the "normal" non-fatal overestimation, where both values are positive and a net gain is still achieved, which is only smaller then the best possible gain of expecting the true value. Fatal overestimation is included in the loss function by using another weighting factor b $(= 2)$ that replaces a:

$$L(\theta, \hat{\theta}) = |(\theta - \hat{\theta})| * b \tag{1-16}$$

   (In other words: Fatal overestimation is twice as bad as simple underestimation.)

4. **Step IV**: A worst case or fatal underestimation can also be derived from the idea of estimating a zero or negative value, when the true value is actually positive. This is assumed to be worse than non-fatal overestimation, but clearly better than fatal overestimation. No already owned resources are wasted, it is only the potential value that is lost, i.e. opportunity costs that arise from completely discarding a reservoir with a potential gain equal to the positive true value. Fatal underestimation is weighted using a third factor c:

$$L(\theta, \hat{\theta}) = |(\theta - \hat{\theta})| * c \tag{1-17}$$

Combining these adaption steps and the conditions defined in them, results in the following customized loss function:

$$L(\theta, \hat{\theta}) = \begin{cases} |\theta - \hat{\theta}|, & \text{for } 0 < \hat{\theta} < \theta \\ |\theta - \hat{\theta}| * a, & \text{for } 0 < \theta < \hat{\theta} \\ |\theta - \hat{\theta}| * b, & \text{for } \theta \leq 0 < \hat{\theta} \\ |\theta - \hat{\theta}| * c, & \text{for } \hat{\theta} \leq 0 < \theta \end{cases}, \text{ with } a, b, c \in \mathbb{Q} \tag{1-18}$$

It is important to note that the weighting factors defined above can take basically any numerical values but should be chosen in a way that they appropriately represent the framework conditions of the problem. Here, based on the considerations named above, it is assumed that normal overestimation is 25% ($a = 1.25$), fatal overestimation 100% ($b = 2$) and fatal underestimation 50% ($c = 1.5$) worse than normal underestimation.
It has to be emphasized that this is just one possible proposal for loss function customization. There exists not one perfect design for such a case. Slight to strong changes can already be implemented by simply varying the values of the weighting factors *a, b* and *c*. Fundamentally different loss functions can also be based on a significantly different mathematical structure. Loss functions are customized regarding the problem environment and according to the to the subjective needs and objectives of an actor. Thus, they are mostly defined by the actor expressing his perspective. Changes in the individual's perception and viewpoint might lead to further customization needs even later on. (Especially considering individual persons as actors, psychological aspects may play a significant role.)

(Estimate or prediction? True value only known if a "yes"-action (development) is taken.)
INSERT PLOTS BASED ON EXAMPLE NORMAL FUNCTIONS?

1-4-1 Including different risk-affinities in the loss function

One can assume that several actors in one sector or decision environment may have the same general loss function, but different affinities concerning risks. This might be based for example on the different psychological factors or economic philosophies followed by companies. It might also be based on budgets and options such actors have available. An intuitive example is the comparison of a small and a large company. A certain false estimate or error might have a significantly stronger impact on a company which has a a generally lower market share and only few projects, than on a larger company which might possess a higher financial flexibility and for which one project is only one of many development options in a portfolio.
In the following, the loss function is further adapted to consider different risk-affinities of several actors. Representing risk behavior in a loss function can also be done in different ways and regarding different types of risks. Here, bidding lower is considered the cautious, risk-averse option, as smaller losses can be expected from underestimating. Guessing higher is deemed riskier, as losses from overestimation are greater. However, bidding correctly on a higher value, will also return a greater gain. It is assumed that risk-friendly actors care less about fatal underestimation, i.e. they will rather develop a project than discard it. In the

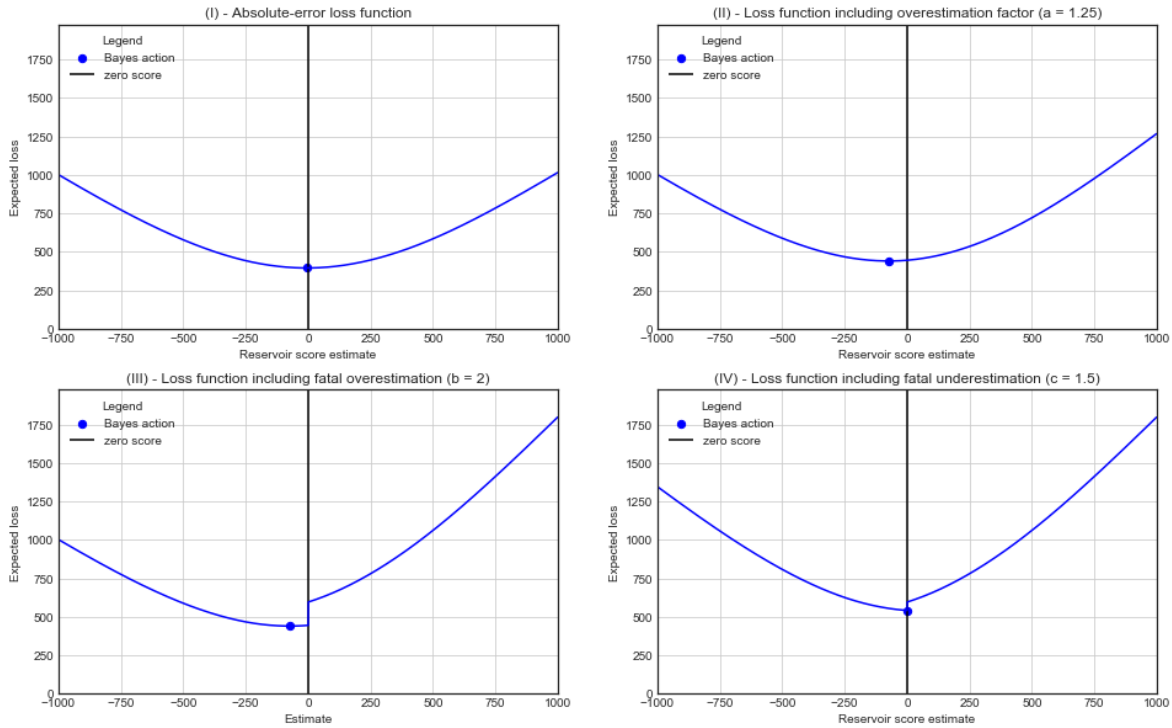

Figure 1-8: The single steps of customizing the loss function are depicted in plots I to IV.

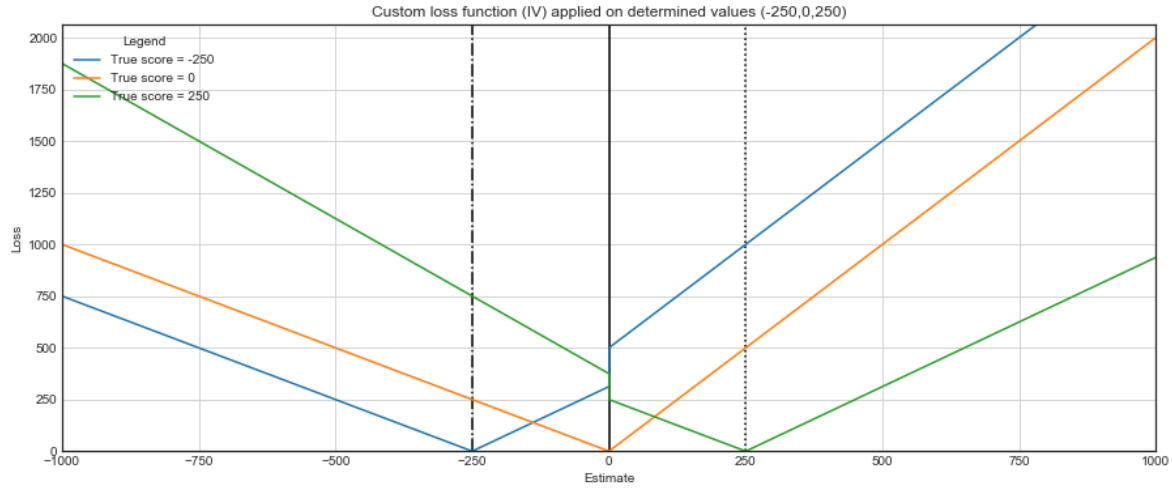

Figure 1-9: Loss based on the customized loss function (Equation 1-18) for determined true scores of -750, 0 and 750.

loss function, risk is simply included using a risk factor r which alters the weighting factors a, b and c respectively:

$$L(\theta,\hat{\theta}) = \begin{cases} |\theta-\hat{\theta}|, & \text{for } 0 < \hat{\theta} < \theta \\ |\theta-\hat{\theta}| * (a * r), & \text{for } 0 < \theta < \hat{\theta} \\ |\theta-\hat{\theta}| * (b * r), & \text{for } \theta \leq 0 < \hat{\theta} \\ |\theta-\hat{\theta}| * (c * (r^{-0.5})), & \text{for } \hat{\theta} \leq 0 < \theta \end{cases}, \text{ with } a,b,c,r \in \mathbb{Q} \tag{1-19}$$

According to this, for $r = 1$ the risk-neutral loss function is returned, since a, b and c are

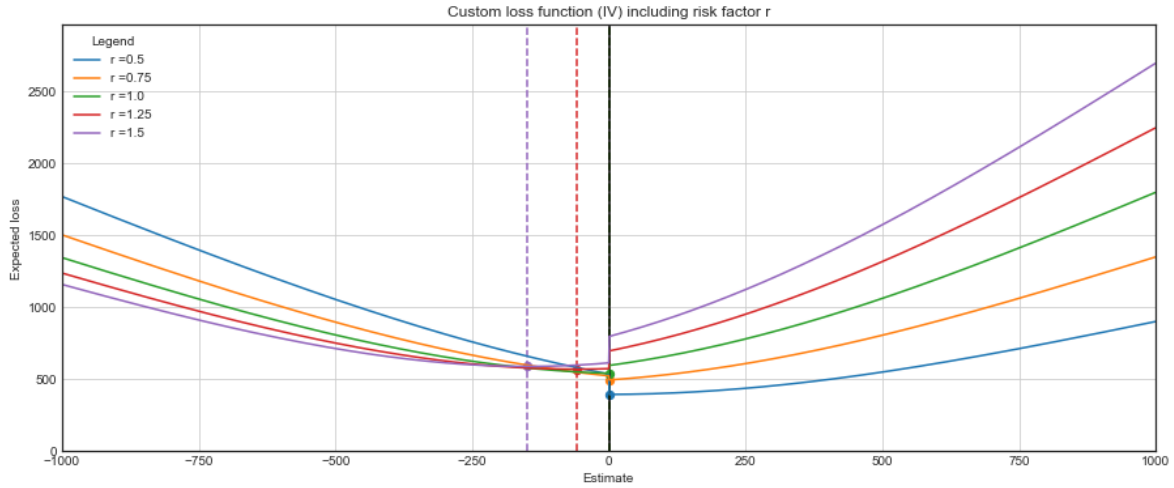

Figure 1-10: Plotting of expected loss realizations after including the risk factor r in the loss function (Equation 1-19) for actors with risk-affinities ranging from risk-averse (r = 0.5 and 0.75), over risk-neutral ($r = 1$), to risk-friendly (r = 1.25 and $r = 1.5$).

not changed. For $r < 1$, the weight on overestimating (a, b) is reduced and increased for fatal underestimation (c). This represents a risk-friendlier actor that is willing to bid on a higher estimate to attain a greater gain. For $r > 1$, the overestimation weight (a, b) is increased in the loss function, the fatal underestimation weight (c) is decreased and respectively more risk-averse actors are prompted to bid on lower estimates.
The factor r can take basically any positive values. However, since risk-neutrality is expressed by $r = 1$, values $0 < r < 2$ are considered to be the most appropriate choices to represent both sides of risk-affinity equally here.

1-5 1D geological reservoir modeling

For simple understanding and a preliminary assessment of the Bayesian statistical methods and the loss function described above, they are first to be applied in the context of an conceptual one-dimensional reservoir case. The underlying model and basic approach are inherited from De la Varga and Wellmann (2016). Parameters are adapted to more appropriately represent a reasonable geological petroleum system, consisting of a reservoir formation with overlying seal in the subsurface. In this 1D setting, only the interface depths and thicknesses of layers such as the reservoir or seal unit can be observed. Other defining aspects, such as

structural entrapment, are assumed to be given. Limiting the model to only one dimension and a small number of uncertain stratigraphical parameters allows for a relatively straightforward and simplified approach to assessing an abstract type of value for a reservoir, applying the custom loss function (Equation 1-18) for value estimation and observing respective effects of Bayesian inference. The construction of the 1D geological model is described in the following.

1-5-1 Construction of the 1D geological model

De la Varga and Wellmann (2016) constructed a simple geological model using three uncertain positions in vertical one-dimensional space, marking hypothetical boundaries of layers in a subsurface column. The location probabilities for these points are defined by sampling from normal distributions. Standard deviations of these distributions increase with depth, representing an increase in uncertainty. For an approximate representation of a hydrocarbon reservoir system, the distribution means were set to depths of 2000 m (seal top), 2050 m (reservoir top) and 2200 m (reservoir bottom). STD-DEVIATIONS? These points confine two layers in the middle, from which the upper one can be labeled as seal and the lower one as reservoir. The resulting model with its prior distributions of possible layer boundary locations is illustrated in Figure **??**.

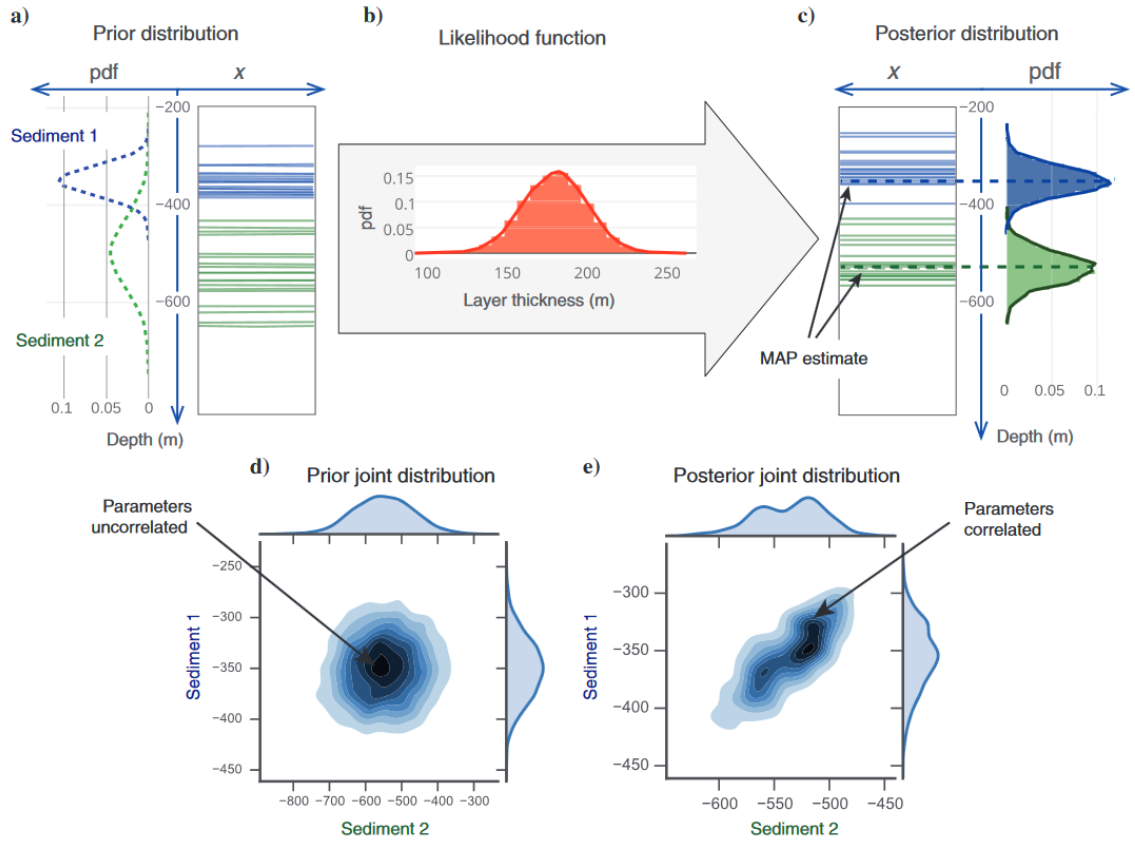

Figure 1-11: (from De la Varga and Wellmann (2016)).

1-5-2 Bayesian inference and analysis of the 1D case

For conducting Bayesian inference, layer thickness likelihood functions are introduced based on another set of normal probability distributions. These are directly related to the layer boundary positions, i.e. the prior distributions. Means and standard deviations of the likelihood distributions are variable, so that several scenarios based on the assumption of different observations can be tested. Parameter priors and likelihood functions are embedded into a probabilistic modeling framework as described in Section 1-2-3 and MCMC sampling is executed accordingly. Posterior distributions can then be evaluated, based on the valuation method described in the following.

1-5-3 Abstract valuation of the 1D geological model

For valuating a simplified 1D model, $OOIP$ and recoverable volume calculations are not applicable, as these require a 3D setting. Given only layer boundary positions in one vertical dimension, it is resorted to an abstract way of reservoir valuation by defining a scoring system. A dimensionless reservoir score is made dependent on three uncertain parameters which can be deduced from the 1D interface positions: (1) reservoir thickness, (2) reservoir top depth and (3) seal thickness (see Figure 1-12).

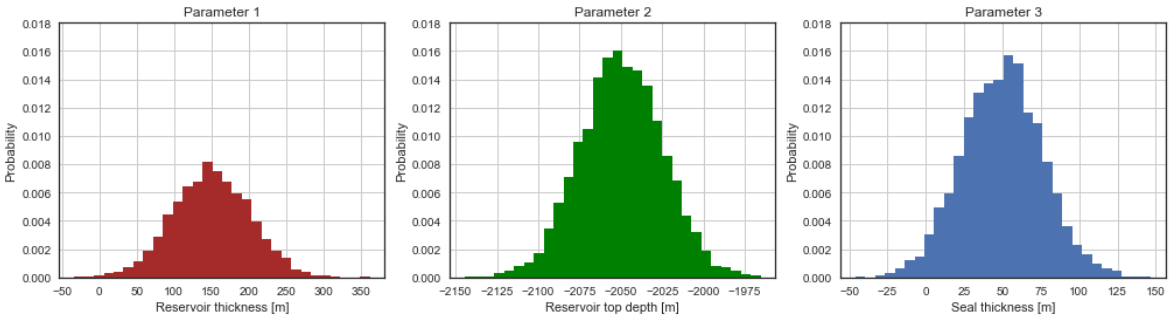

Figure 1-12: Probability distributions for the three parameters deduced from the 1D model depicted in **??**. Values from these parameter distributions are combined in 1-20 attain a score to valuate reservoir model realizations.

Assuming that reservoir thickness is a simplified indicator for the amount of extractable oil or gas and thus value in place, a gain in score can be correlated with increase in thickness. Here, two score points are assigned to one meter of thickness. Increasing costs of drilling are indicated by increasing depth of the reservoir top. Consequently, one negative score point is ascribed to every meter in depth. Samples from the probability distributions of these two parameters are drawn to model the true score of the reservoir (depth scores are subtracted from reservoir thickness scores). A third parameter is defined by the seal thickness. Score points are not added or subtracted by this parameter directly. Instead, a threshold for seal reliability is defined beforehand. Here it is set at 20 m thickness. If the seal thickness falls below this threshold, it is assumed that the seal fails completely and thus all the potential value (positive score) of the reservoir is lost, while costs of depth (negative score) remain. Thus, a condition to check whether the seal is reliable is included in the model. A respective equation for the reservoir score S_{res} is defined as:

$$S_{res} = \begin{cases} 2h_{res} + d_{res}, & \text{for } h_{seal} >= 20 \\ d_{res}, & \text{for } h_{seal} < 20 \end{cases}, \tag{1-20}$$

where reservoir thickness is given by h_{res}, seal thickness by h_{seal} and reservoir depth, which is always a negative value, by d_{res}.
This valuation method is applied on the original prior-only 1D model as reference and then on each posterior distribution set after conducting Bayesian inference. Resulting score probability distributions can be compared directly and additionally under use of the case-specific custom loss function (Equation 1-19) defined before.

1-6 3D geological reservoir model

The concept of the 1D geological model is to be transferred and extended to a 3D setting that incorporates a more complete geological reservoir system. A three-dimensional space allows not only for better consideration of stratigraphical aspects, but also for the inclusion of structural formations, in particular hydrocarbon trap-defining features.

1-6-1 Design of the 3D geological reservoir model

For the purpose of exploring the effect of the methods of Bayesian analysis and decision theory in this work, the model is nevertheless to be kept conceptual and relatively simple. Stratigraphically, it is designed to include one main reservoir unit (sandstone), one main seal unit (shale), an underlying basement through which hydrocarbon fluids could have flown upwards and overlying formations that are assumed to be permeable, so that hydrocarbons can leak upwards. Structurally, it is constructed to feature an anticlinal fold that is displaced by a normal fault. All layers are tilted so that they dip in the opposite direction of the fault plane dip. The original concept of this model is designed in a way, that a potential hydrocarbon trap is formed in the reservoir rock enclosed by the deformed seal and the normal fault.
This trap, more specifically the trap volume, is defined as the central feature of economic interest. For conducting simple and straightforward volumetric calculations, it is assumed that found closed traps are always filled to spill, i.e. the complete trap volume is hydrocarbon filled and the $OOIP$ is attained over this volume.
The maximum trap volume is assumed to equate the hydrocarbon-filled rock volume $A * h$ in Equation 1-12. $OOIP$ and recoverable oil volumes are thus to be used to valuate each realization of the geological model. Single results are expected to vary, depending on the uncertain input parameters defined in Section 1-6-2 below. The custom loss function 1-19 is to be applied on the resulting value distributions before and after performing Bayesian inference. This way, the effect of incorporating additional information in the form of likelihoods is to be assessed from a perspective of Bayesian decision theory. - (to bring this Bayesian method of using loss functions closer to the traditional application of deterministic decision-making in decision-trees, the continuous estimation space of the reservoir value (volume) is combined with the assumption, that the estimated value is linked to a consequent investment into a determined project development size. thus, the continuous approach is used to make the decision in a deterministic decision-making space.)?

1-6-2 Construction of the uncertain 3D geological reservoir model

The 3D structural geological model is constructed as follows: In principle, it is defined as a cubic block with an extent of 2000 m in X, Y and Z directions. The basic input data for the interpolation of the geological features is comprised of 3D point coordinates for layer interfaces and fault surfaces, as well as measurements that indicate respective dip directions and angles. In a Python environment, the data is imported as comma-separated values (CSV) using GemPy. From the generated data frame, GemPy is able to interpolate surfaces following the potential-field method explained in Section 1-2-2 and compute voxel-based 3D geological models (see Figure 1-13).

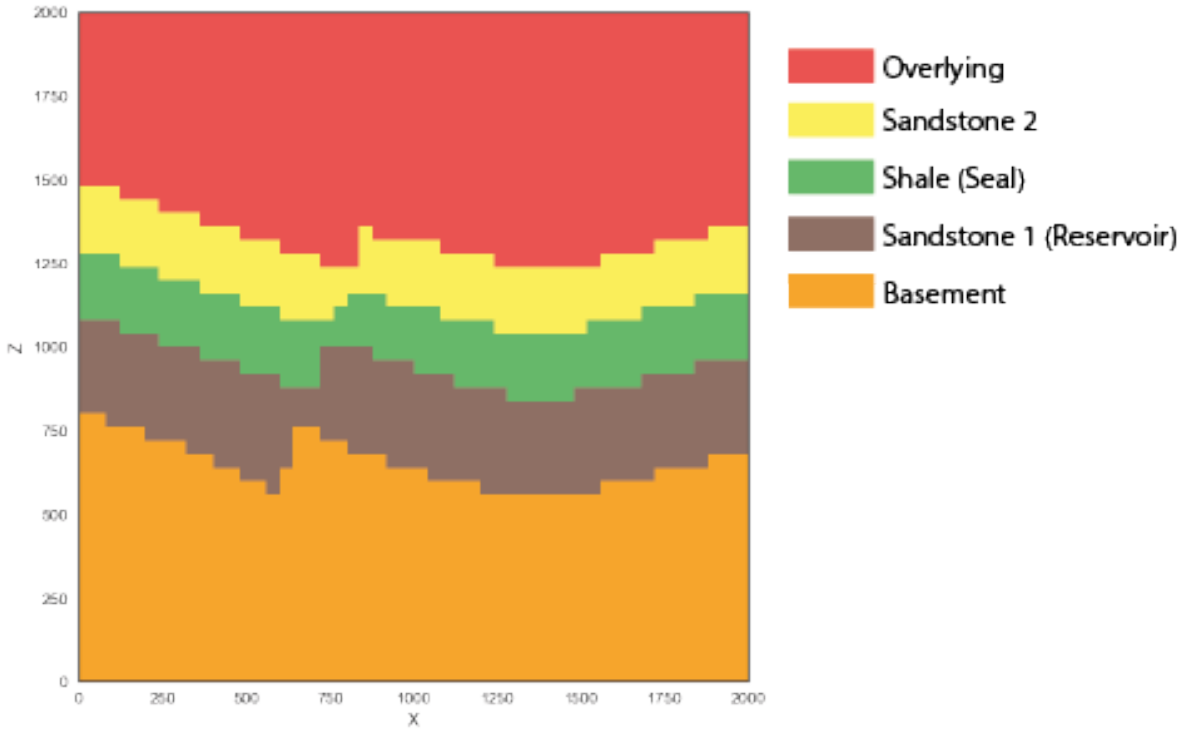

Figure 1-13: Mid section of the base 3D geological model as defined by the original data frame (see Appendix). Layer interfaces are defined by points and foliation dipping indicated by perpendicularly oriented arrows.

Uncertainties are implemented in several ways:

1. **Z-values for layer interfaces:** Analogously to the 1D model, uncertainties for the vertical position of layer interfaces are implemented by using normal probability distributions. A deviation from the original input data Z-value is hereby added and allows for the consideration of uncertainties regarding layer surface positions in depth, layer thicknesses, topological shape and degree of fault offset. Points belonging to the same layer interface are assigned the same base uncertainty by applying one shared probability distribution. Assuming an increase of uncertainty with depth, standard deviations for the distributions are increased for lower formations. Furthermore, uncertainty regarding the magnitude of fault offset is incorporated by adding a further normal probability

distribution that is shared by all layer interface points on the hanging wall. The specific ditributions are listed in the Appendix.

2. **Cross-fault sealing:** Uncertainty about the sealing capacity across the fault is implemented using a Bernoulli distribution. In doing so, a probability of success is defined beforehand. In the case of such a "success", a value of one is returned by the distribution and lateral sealing of the fault is assumed. Should a value of zero be returned, cross-fault leakage is determined to be generally possible, depending on the occurrence of juxtapositions.

3. **Other non-structural parameters:** Other factors that determine the $OOIP$ and ROV calculations, such as porosity and recovery factor, can be implemented stochastically or deterministically. WHAT DO I USE?

1-6-3 Determination of the trap volume

In the course of this work, several algorithms are developed within the Python environment, that in combination enable the automatic recognition and calculation of trap volumes in geological models computed by GemPy. To assign voxels of the model to the trap volume, it is checked whether the following conditions are satisfied by each particular voxel:

1. **Labeled as reservoir formation:** The voxel has been assigned to the target reservoir formation in the lithology block model. This is determined by respective labeling of the input data and the computation conducted by gemPy.

2. **Location in footwall:** The voxel is located on the footwall side of the fault. This condition is applicable to this specific model design, in which entrapment is assumed to occur between the footwall anticlinal enclosure and the normal fault. Due to respective dip of the reservoir formation, full leakage is assumed for the reservoir formation in the hanging wall. A distinction between foot- and hanging wall is easily achievable by using the fault model block that is generated by gemPy. In this fault block, voxels on both sides are assigned respective values for distinction.

3. **Location above spill point horizon:** The voxel is located vertically above the final spill point of the trap. In the algorithm to find this final spill point, it is distinguished between a spill point defined by the folding structure, referred to as anticlinal spill point, and a cross-fault leak point, that depends on the magnitude of displacement and the resulting nature of juxtapositions. Once both of these points have been determined, the higher one is defined to be the final spill point used to determine the maximum fill capacity of the trap. In the case of fault sealing, however, the cross-fault leak point is discarded as irrelevant. Given a juxtapostion with layers overlying the seal, due to fault displacement, the respective section is checked for fault sealing by taking into account the Shale Smear Factor value. The processes of finding the decisive spill point, as well as the determination of juxtapostions and SSF is explained below in further detail.

4. **Location inside of closed system:** The voxel is part of a model section inside of the main anticlinal feature. All of the voxels in this section are separated from the borders of the model by voxels that don't meet the conditions above, which primarily

means that they are encapsulated by seal voxel laterally and upwards. This condition is applicable under the assumption, that connection to the borders of the model lead to leakage. A trap is thus defined as a closed system in this model. It has to be emphasized that these conditions have been fitted to the geological model constructed as described in Section 1-6-2. For other models featuring different geological properties, features and levels of complexities, these conditions might not apply at all or might have to be adapted. Models of higher complexities will surely require the introduction of further conditions.

1-6-4 Finding the final spill point of a trap

Regarding dome-shaped anticlinal structures, it can be observed that, geometrically and mathematically, a spill point is a saddle point of the reservoir top surface in 3D. This was observed by Collignon et al. (2015), who pointed out that the linkage of folds is given by saddle points. These are thus a controling factor for spill-related migration from respective structural traps. For anticlinal traps, closure can consequently be defined as the distance between the saddle point (i.e. spill point) and maximal point of the trap (Collignon et al., 2015).
Regarding a surface defined by $f(x, y)$, a local maximum at (x_0, y_0, z_0) would resemble a hill top (Guichard et al., 2013). Local maxima will be found looking at the cross-sections in the planes $y = y_0$ and $x = x_0$. Furthermore, the respective partial derivatives (i.e. gradients) $\frac{\delta z}{\delta x}$ and $\frac{\delta z}{\delta y}$ will equal zero at x_0 and y_0, i.e. that the extremum is a stationary point (Guichard et al., 2013; Weisstein, 2017). In the context of a geological reservoir system, such a hill can be considered to represent an anticlinal structural trap. Local minima are defined analogously, presenting local minima in both planes at a stationary point (Guichard et al., 2013). A saddle point, however, is a stationary point, while not being an extremum (Weisstein, 2017). In general, saddle points can be distinguished from extrema by applying the second derivative test (Guichard et al., 2013; Weisstein, 2017): Considering a 2D function $f(x, y)$ with continuous partial derivatives at a point (x_0, y_0), so that $f_x(x_0, y_0) = 0$ and $f_x(x_0, y_0) = 0$, the following discriminant D can be introduced:

$$D(x_0, y_0) = f_{xx}(x_0, y_0) f_{yy}(x_0, y_0) - f_{xy}(x_0, y_0)^2 \tag{1-21}$$

Using this, the following holds for a point (x_0, y_0):

(a) If $D > 0$ and $f_{xx}(x_0, y_0) < 0$, there is a local maximum.

(b) If $D > 0$ and $f_{xx}(x_0, y_0) > 0$, there is a local minimum.

(c) If $D < 0$, there is a saddle point at the point (x_0, y_0).

(d) If $D = 0$, the test fails (Guichard et al., 2013).

Figure 1-14 can be seen as a representation of a point of spill between two dome structures (i.e. surface maxima or "hills") which is defined by the surface's saddle point between both.
In gemPy, layer boundary surfaces are returned in the form of discretized arrays of simplices and vertices. The latter can be transformed into a 2D rectangular array that contains Z-positional values for the surface in X and Y directions. According to Verschelde (2017), a saddle point in a matrix is maximal in its row and minimal in its

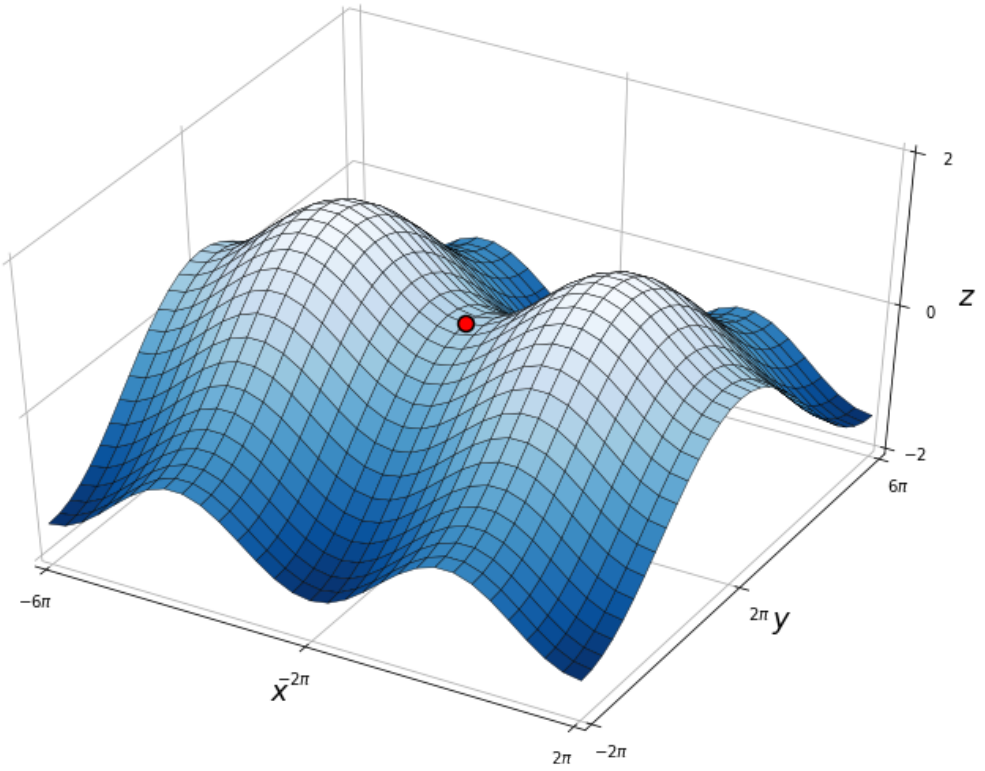

Figure 1-14: Saddle point (red dot) between two maxima. In a geological setting, these surface maxima may be interpreted as two dome-shaped four-way closure traps.

column. This corresponds to the logical geometrical deduction, that a saddle point for a surface defined by $f(x, y)$ is marked by a local maximum in one plane, but a local minimum in the perpendicular plane. This is observable in Figure 1-15.

Regarding leakage across the normal fault in this geological model, a similar approach is taken. If the fault offset remains small enough, that the seal layer is not broken, then the reservoir top surface can be used to find the cross-fault leak point. In this case, the leak point can be defined as the maximal point of hanging wall contact of the reservoir top surface with the fault. At the same time, this point will be a local minimum on the plane perpendicular to the normal fault and thus equal a saddle point. However, higher magnitudes of fault displacement can lead to breaking of the seal, i.e. the juxtaposition of the trap structure with overlying formations which are assumed to be complete permeable. In this case, the maximum footwall contact of the surface with the fault is to be defined as cross-fault leak point.

Following these observations, the algorithm developed in this work uses differentiation techniques to find local extrema in the 2D reservoir top surface arrays attained over gemPy. Points where minima and maxima of perpendicular axes X and Y coincide are then defined as saddle points. The anticlinal spill point is deduced as the maximal saddle point in the footwall. The cross-fault leak point is determined analogously in the hanging wall. In the end, whichever point of these two is maximal, is defined to be the final spill point of the trap. If no cross-fault leak point is found, it is presumed

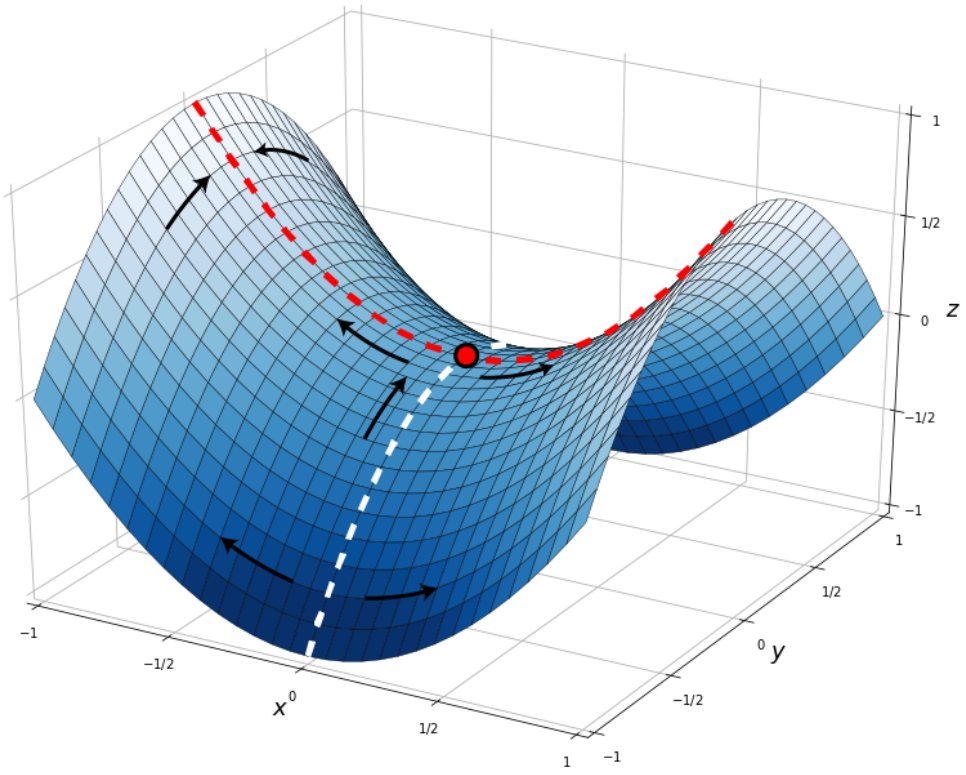

Figure 1-15: Surface and saddle point (red dot) generated by the function $z = x2 - y2$. Maxima in direction y is marked by a red, minima in direction x by a white dashed line. Considering the surface as a seal, consequent buoyant flow directions are indicated by arrows. Such flow would be directed away from minima and towards maxima, with the saddle point indicating a junction and divide, i.e. a possible spill point.

that full leakage is allowed to take place due to little displacement of the reservoir layer. However, if fault sealing is given, any fault leakage and respective leak points become irrelevant and only the anticlinal spill point is considered. The Z-value of the final spill point is used to determine the maximum down-to-horizon to which the trap feature can be filled. Kuijper (2004) has pointed out that using finding spatial critical points, saddle points especially, can be problematic using discretized methods and rectangular grids in particular. Finding all extrema and saddle points can be difficult (Kuijper, 2004). Some failures to detect saddle points in this work's model are resolved by adding a buffer around extrema that define the anticlinal structure. IMPLEMENT BETTER METHOD? However, it has to be pointed out that saddle points might still be missed in some rare cases, especially if they are located in an orientation which is "rotated" and not aligned with the X and Y axes. Furthermore, in this work, the geological model was designed in a way that saddle points are presumed to only occur within or near the structures of interest. FUTURE: MORE UNIVERSALLY APPLICAPLE METHODS

1-6-5 Checking for juxtapositions and possible fault sealing

1-6-6 Calculating the maximum trap volume

Have all voxels that fulfill the conditions defined above been determined, these voxels are seen as part of the maximum trap volume V_{trap}. This volume can then be calculated by simply counting the number of these voxels and rescaling their cumulative volume depending on the resolution in which the model was computed:

$$V_{trap} = n_v * (\frac{S_{orig}}{R_m})^3 \tag{1-22}$$

Where n_v is the number of trap voxels, S_{orig} gives the original scale and R_m the used resolution for the model. As mentioned before, V_{trap} is assumed to equal the hydrocarbon-filled rock volume $A * h$ used in Equation 1-12. For the example of a geological model with an original extent of 2000 m in three directions, computed using a resolution of 50, the scale factor is 40 m. Every voxels thus accounts for $40^3\ m = 64,000\ m^3$ in volume. It has to be noted, that this direct approach to rescaling and calculating the volume requires the model to be designed as a cubic block.

1-6-7 Implementation of reservoir-related likelihoods in the 3D model

As for the 1D case before, for the 3D case it is assumed that additional information is provided in the form of layers thickness likelihoods. In this geological scenario, the information might have been gained for example from additional seismic observations or from core sample data from a well nearby. Likelihoods could also be derived from knowledge of the geological history of the formation, such as the depositional environment of sedimentary layers. Assuming a possible correlation of nearby core samples with the layers in our model section, layer thickness likelihoods can be deduced respectively. First of all, a method to determine layer thicknesses in our model realizations has to be introduced. Here, as single X- and Y-point (1D column in Z) in the footwall of the model is chosen as a measure for the thickness of the layers. In this column, point coordinates for the layer interfaces had been defined in the original data frame and can be observed as they are altered in the interpolation data frame for each iteration. The column is located centrally in the overall model block, as well as the original potential trap structure (X = 1100 m,Y = 1000 m) and is thus presumed to be representative and of significance for the reservoir analysis. Thickness variations are traced and vary relative to the changes in the layer interface positions, given by their uncertainties in Z-values.

After defining these thickness to point-positional dependencies, thickness likelihoods are implemented as probability distributions, as done for the 1D model. Various types of geological information, conclusions and expectations can be expressed by adapting mean and standard deviation of these normal distributions. For core sampling, for example, information might be evenly provided for all layers, irrespective of depth, so that similar standard distributions might be assigned to all layer thicknesses. Alternatively, taking into account certain depositional environments for which high thickness

variablity is characteristic, specific standard deviations can be raised accordingly. Some representative cases are presented in Chapter 2.

1-6-8 Bayesian analysis and valuation of the 3D model

According to the methods introduced in Sections 1-1 and 1-2, the 3D geological model is to be incorporated in a probabilistic modeling framework and analyzed from a Bayesian perspective.

First, a simple Monte Carlo error propagation run, using only priors, is conducted so that reference distributions

Chapter 2

Results

Text

2-1 1D geological reservoir model results

2-1-1 Scoring

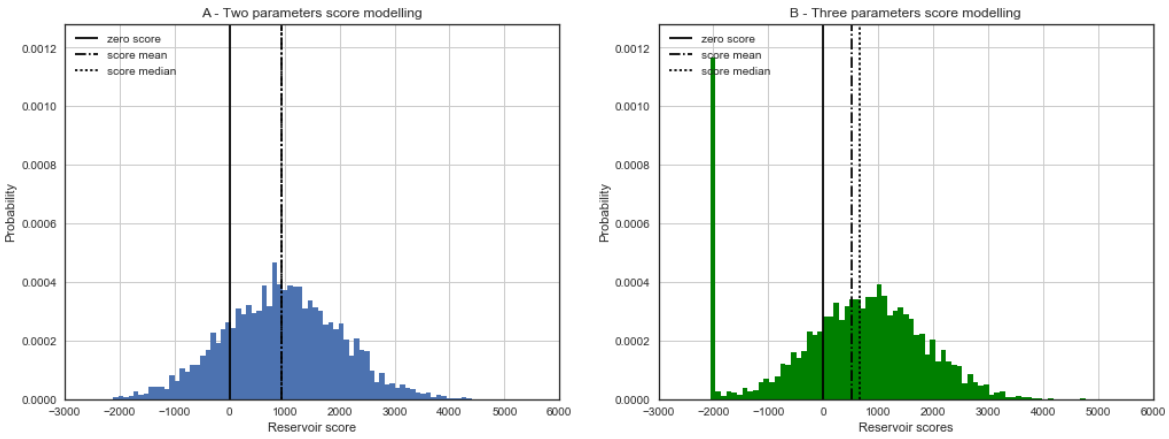

Figure 2-1: Posterior probability distributions from modeling scores using two (A) and three parameters (B).

Results from scoring based on a 1D model constructed as defined in Section 1-5-1 are plotted in Figure 2-1. A test run of scoring with only the two parameters reservoir thickness and depth, is shown in 2-1-A. These results represented by an approximately normal distribution. The score is negative in about 17% of the cases. Mean and median are about the same.
Full scoring results, including also seal reliability as a parameter, are visualized in Figure 2-1-B. The main distribution is not changed significantly, except for a striking peak of

probability at the possibility for a score of -2000. This presumably represents the bulk of cases, in which the seal was assumed to have failed. It is to be noted, that the mean of the seal top distribution is found at -2000 m. It can be seen in Figure **??**, that around that depth in the model column, reservoir top and seal top probability distributions significantly overlap. Thus, there is a possibility for a higher score, due to a shallower reservoir top position, but also a high probability for a seal that is to thin to be reliable. The negative score peak at -2000 is thus presumably caused by a high number of seal failures, due to both layer tops found in this area. Furthermore, mean and median of the score distribution have been shifted to lower values and are now found further apart.

2-1-2 Applying the custom loss function on the 1D reservoir scores

Realizations of the four loss function adaption steps as elaborated in Section 1-4 and based on the scoring results shown in Figure 2-1-B are depicted in the plots in Figure **??**. As expected, the median is returned for the Bayes action, when using the standard symmetric absolute-error loss function (Figure **??**-I). Compared to this, it can be observed that assigning a stronger weight on overestimation (Figure **??**-II) steepens the curve on the right hand side and shifts the minimum to the left, i.e. to a lower estimate. Using $a = 1.25$, the Bayes action changes from the median, to a value close to the mean of the distribution. The shift and steepening are significantly reinforced by the introduction of fatal overestimation (Figure **??**-III). With $b = 2$, the Bayes action drops to the zero score estimate. It can also be noted, that by defining a condition dependent on the algebraic sign of the values, according to which only losses for positive estimates are multiplied by b, a distinct jump appears at the zero score boundary. Due to a similar condition, the same effect is observed on the negative side of estimate values, where the curve has also been steepened, after including fatal underestimation (Figure **??**-IV). This comes with a shift of the minimum towards positive values. It is also to be noted that with every customization step, the overall expected loss is increased.
The implementation of the final custom loss function (Figure **??**-IV) using single determined values for the true score is plotted in Figure 1-9. This helps to clarify the way real losses result for each guess, relative to given true score values. The expected loss is acquired by arithmetically averaging such loss realizations based on the true score probability distribution by using Equation 1-6.
Implementing risk-affinity as a factor r leads to different steepnesses of the plotted curves depicting loss and expected loss. The effect on the latter is visualized in Figure 2-2, where 0.5, 0.75, 1, 1.25 and 1.5 were chosen as values for r. It can be observed that the minima for expected loss, i.e. the Bayesian estimators for differently risk-affine actors, are located at different estimates. Mean and median are clearly surpassed by the best estimate of the most risk-friendly actor ($r = 0.5$), while for the most risk-averse actors ($r = 1.25$ and $r = 1.5$), the Bayes action equals a zero score estimate and thus the decision to take no action. In Figure 2-2 it can also be recognized that the expected loss is generally lower for risk-friendlier actors on the side of positive estimates, which is the relevant side for decision-making.

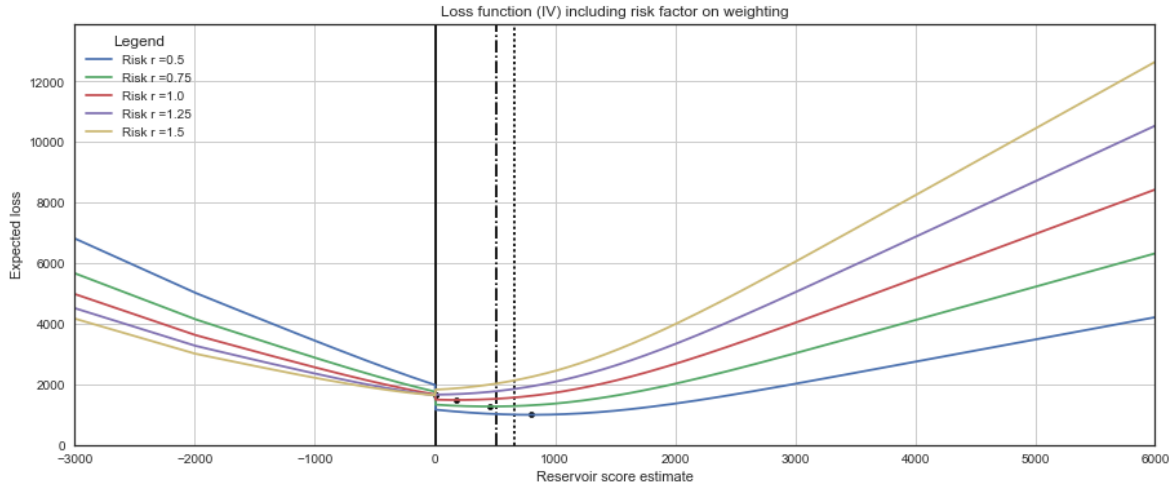

Figure 2-2: Plotting of expected loss realizations after including the risk factor r in the loss function (Equation 1-19) for actors with risk-affinities ranging from risk-averse ($r = 0.5$ and 0.75), over risk-neutral ($r = 1$), to risk-friendly ($r = 1.25$ and $r = 1.5$).

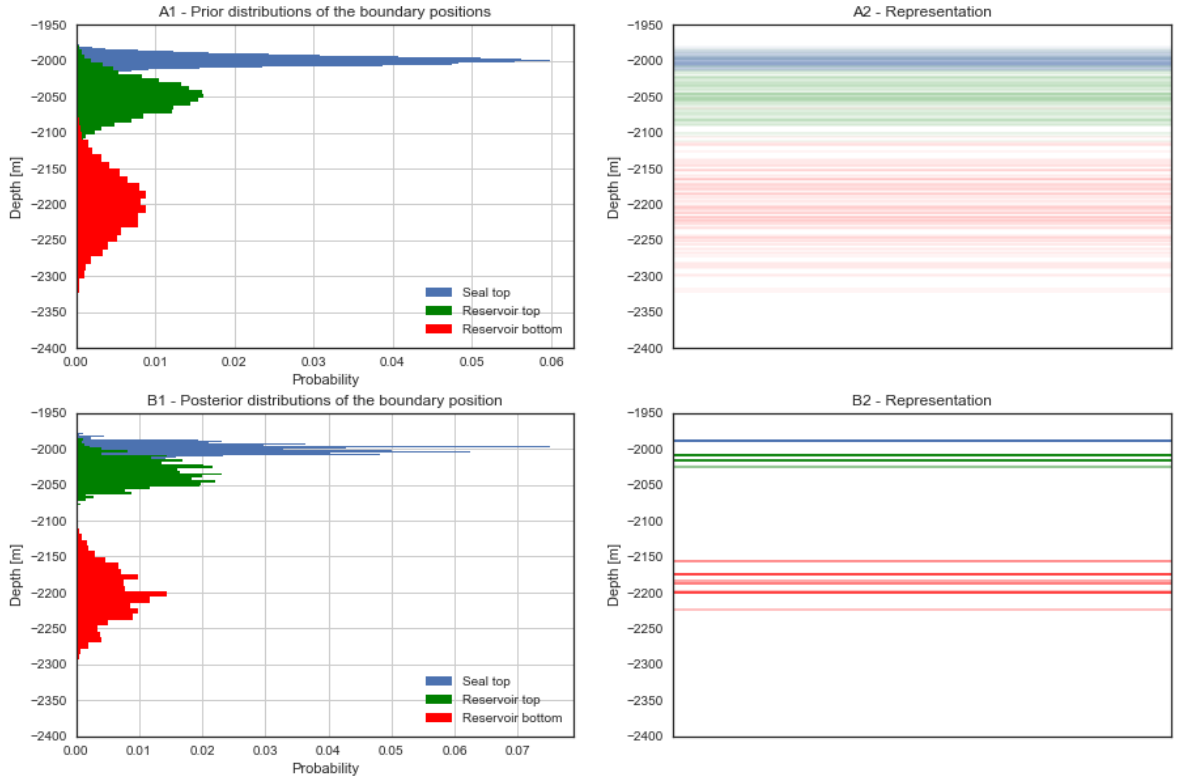

Figure 2-3: Prior (A1) and posterior distributions (A2) of the layer boundary positions in depth and respective representations (A2, B2).

2-1-3 Bayesian updating using thickness likelihoods

De la Varga and Wellmann (2016) made use of Bayesian inference to reduce the uncertainty in this type of one-dimensional model. The same is conducted here in the following.
The probability distributions for the location of the layer boundaries are treated as priors. Now it is assumed that new observations have been made, providing additional information on the likelihoods of the thicknesses of the two layers. Likelihood functions for reservoir and seal thicknesses are introduced in the form of normal distributions, defined by means and standard deviations. These parameters vary according to nature of the observations made. Using the principle of Bayesian inference as explained in Chapter 1-1, the model is updated and new posterior distributions for our true reservoir score are attained
Different Bayesian updating cases with different sets of likelihoods are presented in the following, so that various possible results can be compared. Each take the layer boundaries defined in Section 1-5-1 as priors and use Bayesian inference with respective likelihood data defined below for each case.

Updating case I: Moderately reinforcing information

In this first case, a normal distribution with a mean of 25 m and a standard deviation of 20 m is chosen to reflect the likelihood of the seal thickness. For the reservoir, a normal distribution with a mean of 180 m and a standard deviation of 60 m is chosen. Using these likelihoods to update the 1D geological model, the uncertainty in the posterior probability distributions for the positions of layer boundaries in depth is reduced (see Figure 2-3).
Scoring is applied based on these new distributions. In Figure 2-4-A, it can be recognized that the bulk of the score distribution was shifted to the positive side of values, while the peak at -2000 was raised. The probability of scores between -2000 and 0 decreased significantly, i.e. the true score is most likely either positive or -2000 if it is negative.
Application of the custom loss function (Equation 1-19) is visualized in Figure 2-4, in which the expected losses are compared before (B1) and after (B2) uncertainty reduction. It is observable, that by adding information about layer thickness likelihoods, Bayes actions are shifted relative to the nature of the information. In this case, the added data generally reinforces the probability of the reservoir to be significantly thick. Information on the seal, however, based on a normal distribution around 25 m thickness, leaves uncertainty about the reliability of the seal, as the safety threshold is defined as 20 m.
NOT INCREASED CERTAINTY; ONLY OVERALL VALUES! Increased certainty about the reservoir thickness is sufficient to shift Bayes actions to higher estimates for all actors, but the most risk-averse one ($r = 1.5$). These shifts are quantified in Table 2-1. According to these numbers, the risk-neutral actor's estimate is increased the most, the risk-friendliest actor's estimate the least. Expected losses are decreased for the risk-neutral and the two risk-friendlier individuals. It is clear that the expected loss was reduced the most for the risk-friendliest actor and it increased most significantly

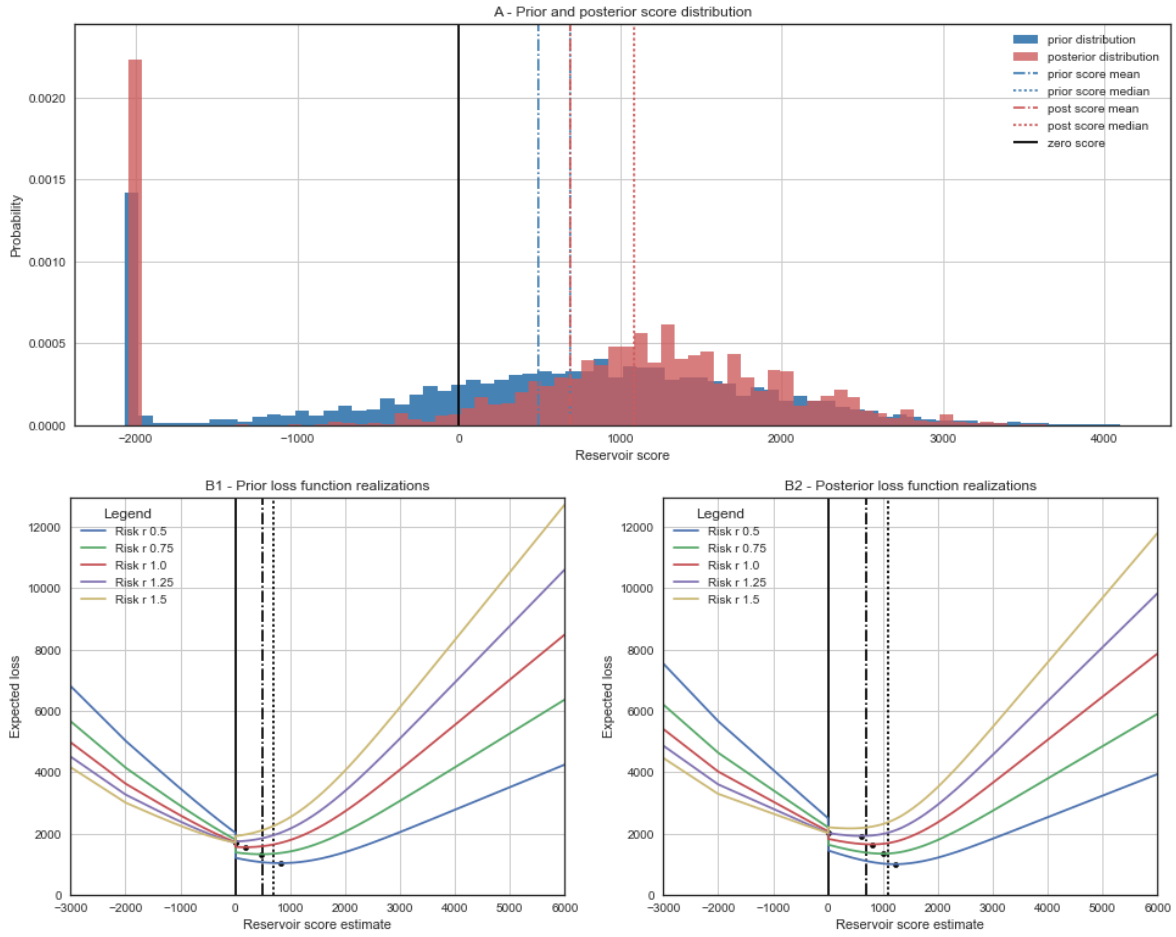

Figure 2-4: Reservoir score distributions (A) and change in the realizations of expected loss for several risk parameters (B1, B2) before and after Bayesian updating based on likelihoods defined as follows: Seal thickness mean = 25 m, std = 20 m. Reservoir thickness mean = 180 m, std = 60 m.

for the most risk-averse actor.

Updating case II: Likely reliable seal

In this second case, the reservoir thickness likelihood is defined in the same way as in case I (mean = 180 m, standard deviation = 60 m). For the seal, a mean of 50 m with a standard deviation of 20 m is chosen, favoring the likelihood of a reliable seal relative to the threshold of 20 m thickness. Respective score results are depicted in Figure 2-5-A. The bulk of the distribution is narrowed on the positive side of estimates. Mean and median are clearly shifted to higher values. The "seal failure peak" at -2000 is significantly decreased.

Applying the custom loss function on this new score distribution results in the realizations of expected loss illustrated in Figure 2-5. Bayes actions are shifted clearly to higher estimates and expected losses of these minima are significantly reduced for

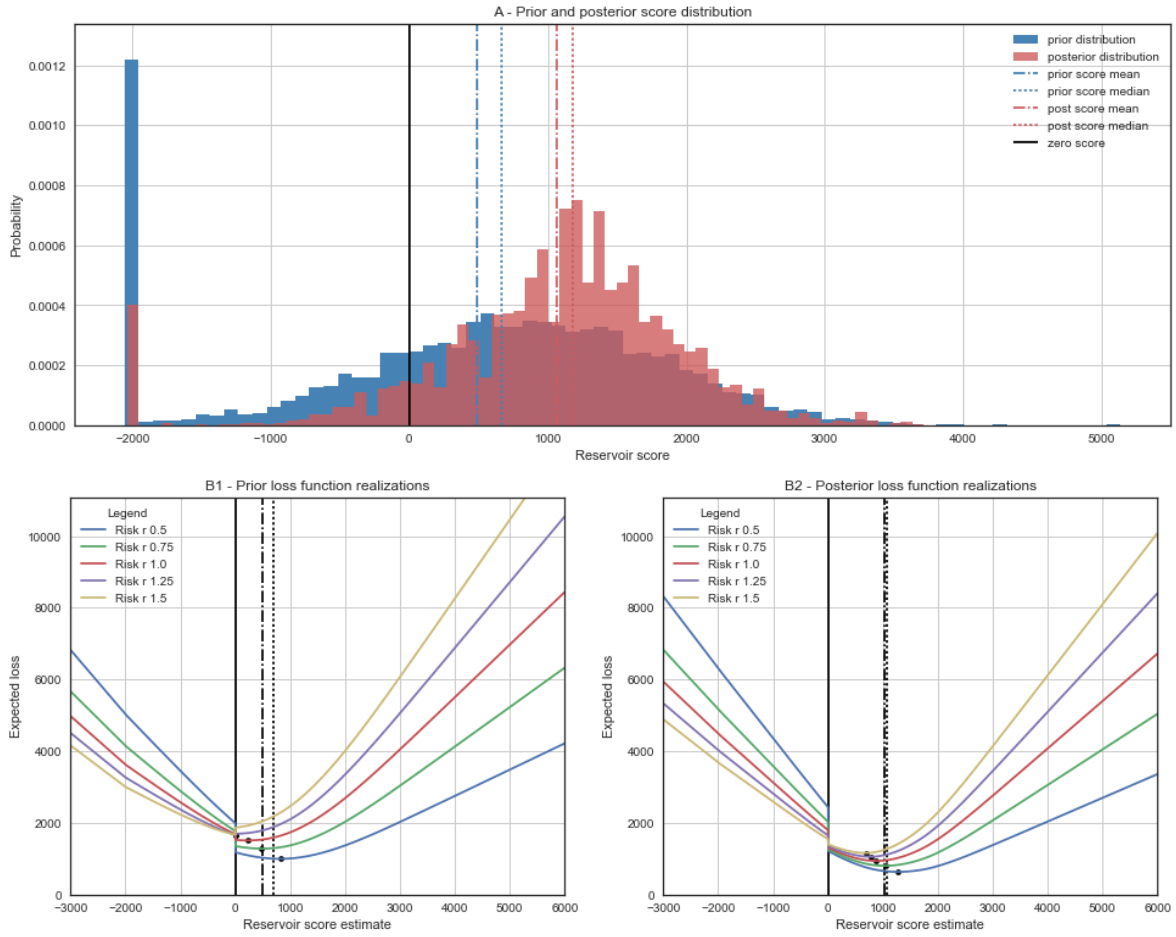

Figure 2-5: Reservoir score distributions (A) and change in the realizations of expected loss for several risk parameters (B1, B2) before and after Bayesian updating based on likelihoods defined as follows: Seal thickness mean = 50 m, std = 20 m. Reservoir thickness mean = 180 m, std = 60 m.

all actors. This is quantified in Table 2-1. According to these values, the risk-neutral to risk-averse individuals seem to profit the most, due to a large change in estimate value and decreased expected loss. Compared to case I, the estimate shifts for both risk-friendlier actors remain approximately the same, expected losses, however, are lowered much more significantly. POINT OUT: DECREASED UNCERTAINTY! AND HIGHER VALUES OVERALL!

Updating case III: Safe seal but likely subpar reservoir thickness

In this third case, seal safety is ensured by using a mean of 70 m with a standard deviation of 10 m for the seal thickness likelihood. However, the new observations are assumed to provide information about the reservoir unit that makes it likely to be thinner than expected. Reservoir thickness likelihood is assigned a mean of 100 m and a standard deviation of 40 m.

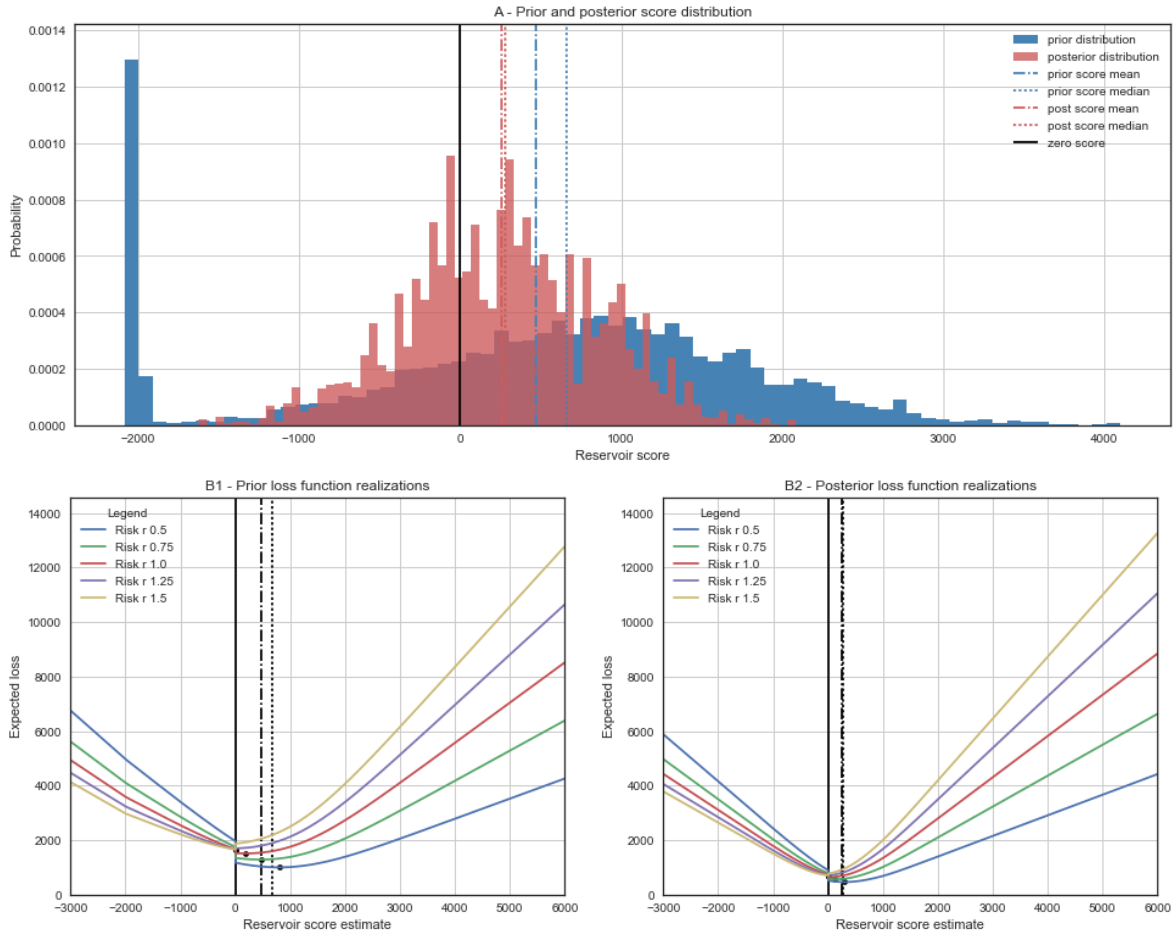

Figure 2-6: Reservoir score distributions (A) and change in the realizations of expected loss for several risk parameters (B1, B2) before and after Bayesian updating based on likelihoods defined as follows: Seal thickness mean = 70 m, std = 10 m. Reservoir thickness mean = 100 m, std = 40 m.

The subsequent score distribution is depicted in Figure 2-6. It can be seen that while the whole distribution is narrowed, it also is shifted to the left, to lower and negative estimates. Mean and median are almost the same. As seal reliability is practically guaranteed, the peak at -2000 m vanishes.

Based on this reservoir score probability distribution, Bayes actions are shifted to lower estimates for all actors using the custom loss function (see Figure 2-6). In fact, all but the most risk-friendly individual ($r = 0.5$) find their Bayesian estimator to be zero now, i.e. project development is deemed to be too risky to them. Furthermore, the spread of expected loss values around the minima for all actors is diminished. In other words, the expected loss values of the Bayes actions are now much closer to each other. Notable is the large reduction of expected loss in general. Quantified changes in the positions and values of the Bayes actions are listed in Table 2-1. There is no shift in estimate for risk-averse actors, as they already found their best estimates to be zero before updating. DECREASED UNCERTAINTY BUT AT THE SAME TIME LOWER VALUES OVERALL!

	Example I		Example II		Example III	
r	Δ BA	Δ EL	Δ BA	Δ EL	Δ BA	Δ EL
0.50	+ 553.67	- 105.49	+ 522.95	- 436.26	- 498.98	- 538.08
0.75	+ 673.40	- 81.67	+ 697.73	- 551.92	- 346.16	- 717.83
1.00	+ 750.05	- 33.56	+ 855.57	- 631.92	- 176.13	- 872.02
1.25	+ 713.19	+ 75.71	+ 912.43	- 647.10	- 0.00	- 946.04
1.50	+ 0.00	+ 282.64	+ 819.26	- 545.96	- 0.00	- 951.57

Table 2-1: Changes in Bayes action (BA) and minimal expected loss (EL) for Bayesian updating cases I, II and III and respective actors with risk parameters r.

NEED TO INCLUDE CLEAR BA VALUES BEFORE AND AFTER!!! NOT VISIBLE IN PLOTS.

2-1-4 General 1D model updating results

It is already shown by these three abstract 1D modeling cases, how Bayesian updating and change in uncertainties affects the way differently risk-affine decision-makers choose best estimates based on the custom loss function (Equation 1-19). As can be expected intuitively, reassurance of positive scores, for example by narrowing of the distribution of scores on the side of positive estimates or by reducing the occurrence of negative extrema, leads to shifts towards higher Bayes action estimates for all actors. Conversely, actors are discouraged to expect gains when facing a higher probability of negative scores. Unsurprising is also the inverse behavior of risk-averse and risk-friendly individuals. However, it is most notable that a reduction of uncertainty in any case leads to a diminished spread of Bayes actions between all actors. In other words, given better information about the true value of the reservoir, different actors come to more similar decisions. Given perfect information, all actors would presumably choose the same estimate, which would equal the true score.

2-2 Results using the 3D geological model

Chapter 3

Discussion

1D CASE:

-abstract case: easy model construction and straightforward design of a loss function making basic assumptions and taking relative values that can simply be exchanged

-so representative in a "relative" way, mostly appropriate to illustrate principles and benefits of the methodology

-decision making/ estimation is defined by the design of the loss function which includes framework parameters which depend on the problem environment (e.g. market, technical constraints, etc.)

-similar actors but different behaviors concerning risk: different decisions but same general loss function path (just different minima of EL)

-additional information changes decision (BA) and EL

-magnitude of change varies not only with the nature of the information (magnitude of uncertainty reduction) but also with the risk parameter

-some actors might benefit more from some specific additional information than others

-quantifiable value of information??

Chapter 4

Conclusion

Bibliography

Aug, C. (2004). *Modélisation géologique 3D et caractérisation des incertitudes par la méthode du champ de potentiel*. PhD thesis, École Nationale Supérieure des Mines de Paris.

Behnel, S., Bradshaw, R., Citro, C., Dalcin, L., Seljebotn, D. S., and K, S. (2010). Cython: The best of both worlds. *Computing in Science Engineering*, 13(2).

Berger, J. O. (2013). *Statistical decision theory and Bayesian analysis*. Springer Science & Business Media.

Calcagno, P., Chilès, J.-P., Courrioux, G., and Guillen, A. (2008). Geological modelling from field data and geological knowledge: Part i. modelling method coupling 3d potential-field interpolation and geological rules. *Physics of the Earth and Planetary Interiors*, 171(1):147–157.

Chilès, J.-P., Aug, C., Guillen, A., and Lees, T. (2004). Modelling the geometry of geological units and its uncertainty in 3d from structural data: the potential-field method. In *Proceedings of international symposium on orebody modelling and strategic mine planning, Perth, Australia*, volume 22, page 24.

Collignon, M., Fernandez, N., and Kaus, B. (2015). Influence of surface processes and initial topography on lateral fold growth and fold linkage mode. pages n/a–n/a.

Davidson-Pilon, C. (2015). Bayesian methods for hackers: Probabilistic programming and bayesian inference.

De la Varga, M. and Schaaf, A. (2017). Gempy. https://github.com/cgre-aachen/gempy/.

De la Varga, M. and Wellmann, J. F. (2016). Structural geologic modeling as an inference problem: A bayesian perspective. *Interpretation*, 4(3):SM1–SM16.

Dean, L. (2007). Reservoir engineering for geologists - volumetric estimation. *The Monthly Magazine of the Canadian Society of Petroleum Geologists*, pages 11–14.

Dolson, J. (2016a). The basics of traps, seals, reservoirs and shows. In *Understanding Oil and Gas Shows and Seals in the Search for Hydrocarbons*, pages 47–90. Springer.

Dolson, J. (2016b). Quantifying seals and saturations: Capillary pressure, pseudo-capillary pressure and quantitative show assessment. In *Understanding Oil and Gas Shows and Seals in the Search for Hydrocarbons*, pages 233–314. Springer.

Færseth, R. B. (2006). Shale smear along large faults: continuity of smear and the fault seal capacity. *Journal of the Geological Society*, 163(5):741–751.

Gelman, A., Carlin, J. B., Stern, H. S., and Rubin, D. B. (2014). *Bayesian data analysis*, volume 2. Taylor & Francis.

Geman, S. and Geman, D. (1984). Stochastic relaxation, gibbs distributions, and the bayesian restoration of images. *Pattern Analysis and Machine Intelligence, IEEE Transactions on*, (6):721–741.

Gilks, W. R. (2005). *Markov chain monte carlo*. Wiley Online Library.

Guichard, D., Koblitz, N., and Keisler, H. J. (2013). *Calculus: Early Transcendentals*. D. Guichard.

Haario, H., Saksman, E., and Tamminen, J. (2001). An adaptive metropolis algorithm. bernoulli 7 223–242. *Mathematical Reviews (MathSciNet): MR1828504 Digital Object Identifier: doi*, 10:3318737.

Hastings, W. (1970). Monte carlo sampling methods using Markov chains and their applications. *Biometrika*, 57(1):97–109.

Hennig, C. and Kutlukaya, M. (2007). Some thoughts about the design of loss functions. *REVSTAT - Statistical Journal*, 5(1):19–39.

Hoffman, M. D. and Gelman, A. (2014). The no-u-turn sampler: Adaptively setting path lengths in hamiltonian monte carlo. *The Journal of Machine Learning Research*, 15(1):1593–1623.

Kuijper, A. (2004). On detecting all saddle points in 2d images. *Pattern Recognition Letters*, 25(15):1665–1672.

Labastie, A. (2011). En route: Increasing recovery factors: A necessity.

Lajaunie, C., Courrioux, G., and Manuel, L. (1997). Foliation fields and 3D cartography in geology: Principles of a method based on potential interpolation. *Mathematical Geology*, 29(4):571–584.

Langtangen, P. H. (2008). *Python scripting for computational science*. Springer Verlag, New York.

Lindsay, N., Murphy, F., Walsh, J., and Watterson, J. (1993). Outcrop studies of shale smears on fault surfaces. *The Geological Modelling of Hydrocarbon Reservoirs and Outcrop Analogues*, pages 113–123.

Metropolis, N., Rosenbluth, A. W., Rosenbluth, M. N., Teller, A. H., and Teller, E. (1953). Equation of state calculations by fast computing machines. *The journal of chemical physics*, 21(6):1087–1092.

Salvatier, J., Wiecki, T. V., and Fonnesbeck, C. (2016). Probabilistic programming in python using pymc3. *PeerJ Computer Science*, 55(2).

Schaaf, A. (2017). Geological inference based on kinematic structural models. Master's thesis, RWTH AACHEN UNIVERSITY, Aachen, Germany.

Schmatz, J., Vrolijk, P., and Urai, J. (2010). Clay smear in normal fault zones–the effect of multilayers and clay cementation in water-saturated model experiments. *Journal of Structural Geology*, 32(11):1834–1849.

Sorkhabi, R. and Tsuji, Y. (2005). The place of faults in petroleum traps.

van der Zee, W. and Urai, J. L. (2005). Processes of normal fault evolution in a siliciclastic sequence: a case study from miri, sarawak, malaysia. *Journal of Structural Geology*, 27(12):2281–2300.

van der Zee, W., Urai, J. L., and Richard, P. D. (2003). Lateral clay injection into normal faults. *GEOARABIA-MANAMA-*, 8:501–522.

Verschelde, J. (2017). Programming tools and file management - part i: A tour of python. http://homepages.math.uic.edu/~jan/mcs275/mcs275notes/index.html. Last visited on 18/10/2017.

Vrolijk, P. J., Urai, J. L., and Kettermann, M. (2016). Clay smear: Review of mechanisms and applications. *Journal of Structural Geology*, 86:95–152.

Weisstein, E. W. (2017). Saddle point. from mathworld—a wolfram web resource. http://mathworld.wolfram.com/SaddlePoint.html. Last visited on 18/10/2017.

Wellmann, J. F., De la Varga, M., Murdie, R. E., Gessner, K., and Jessell, M. (2017). Uncertainty estimation for a geological model of the sandstone greenstone belt, western australia insights from integrated geological and geophysical inversion in a bayesian inference framework. In Gessner, K., Glessinkop, T. G., and Sorjonen-Ward, P., editors, *Characterization of Ore-Forming Systems from Geological, Geochemical and Geophysical Studies*. Geological Society, London, Special Publications, 453.

Yielding, G. (2012). Using probabilistic shale smear modelling to relate sgr predictions of column height to fault-zone heterogeneity. *Petroleum Geoscience*, 18(1):33–42.

Yielding, G., Freeman, B., and Needham, D. T. (1997). Quantitative fault seal prediction. *AAPG bulletin*, 81(6):897–917.

Appendix A

The back of the thesis

A-1 An appendix section

A-1-1 An appendix subsection with C++ Lisitng

```
//
// C++ Listing Test
//

#include <stdio.h>

for(int i=0;i<10;i++)
{
    cout << "Ok\n";
}
```

A-1-2 A Matlab Listing

```
%
% Comment
%
n=10;
for i=1:n
    disp('Ok');
end
```

Appendix B

Yet another appendix

B-1 Another test section

Ok, all is well.